Non-Abelian quantum order in spin-orbit-coupled semiconductors: Search for topological Majorana particles in solid-state systems

Jay D. Sau,[1] Sumanta Tewari,[2,1] Roman M. Lutchyn,[1] Tudor D. Stanescu,[3,1] and S. Das Sarma[1]
[1]*Condensed Matter Theory Center and Joint Quantum Institute, Department of Physics, University of Maryland, College Park, Maryland 20742, USA*
[2]*Department of Physics and Astronomy, Clemson University, Clemson, South Carolina 29634, USA*
[3]*Department of Physics, West Virginia University, Morgantown, West Virginia 26506, USA*
(Received 1 July 2010; revised manuscript received 4 September 2010; published 9 December 2010)

We show that an ordinary semiconducting thin film with spin-orbit coupling can, under appropriate circumstances, be in a quantum topologically ordered state supporting exotic Majorana excitations which follow non-Abelian statistics. The key to the quantum topological order is the coexistence of spin-orbit coupling with proximity-induced *s*-wave superconductivity and an externally induced Zeeman coupling of the spins. For the Zeeman coupling below a critical value, the system is a nontopological (proximity-induced) *s*-wave superconductor. However, for a range of Zeeman coupling above the critical value, the lowest energy excited state inside a vortex is a zero-energy Majorana fermion state. The system, thus, has entered into a non-Abelian *s*-wave superconducting state via a topological quantum phase transition (TQPT) tuned by the Zeeman coupling. In the topological phase, since the time-reversal symmetry is explicitly broken by the Zeeman term in the Hamiltonian, the edge of the film constitutes a *chiral* Majorana wire. Just like the *s*-wave superconductivity, the Zeeman coupling can also be proximity induced in the film by an adjacent magnetic insulator. We show this by an explicit model tight-binding calculation for both types of proximity effects in the heterostructure geometry. Here we show that the same TQPT can be accessed by varying the interface transparency between the film and the superconductor. For the transparency below (above) a critical value, the system is a topological (regular) *s*-wave superconductor. In the one-dimensional version of the same structure and for the Zeeman coupling above the critical value, there are localized Majorana zero-energy modes at the two ends of a semiconducting quantum nanowire. In this case, the Zeeman coupling can be induced more easily by an external magnetic field parallel to the wire, obviating the need for a magnetic insulator. We show that, despite the fact that the superconducting pair potential in the nanowire is explicitly *s* wave, tunneling of electrons to the ends of the wire reveals a pronounced zero-bias peak. Such a peak is absent when the Zeeman coupling is below its critical value, i.e., the nanowire is in the nontopological *s*-wave superconducting state. We argue that the observation of this zero-bias tunneling peak in the semiconductor nanowire is possibly the simplest and clearest experiment proposed so far to unambiguously detect a Majorana fermion mode in a condensed-matter system.

DOI: 10.1103/PhysRevB.82.214509 PACS number(s): 03.67.Lx, 71.10.Pm, 74.45.+c

I. INTRODUCTION

Particle statistics of a collection of indistinguishable particles is a genuinely quantum-mechanical concept without any classical analog. In spatial dimensions three and above, pairwise interchange of particle coordinates in a many-body system is equivalent to a simple permutation of the coordinates. Consequently, each interchange has the effect of either a change in sign (fermion) or no change at all (boson) on the many-body quantum wave function. In (2+1) dimensions, however, exchanges and permutations are not necessarily equivalent.[1–3] In this case, under simple interchange of the particle coordinates, the corresponding space-time trajectories can form nontrivial braids in the (2+1)-dimensional space time.[4] Consequently, in (2+1) dimensions, particles can have quantum statistics strikingly different from the statistics of bosons and fermions.

A straightforward extension of the statistics of bosons and fermions is the Abelian anyonic statistics, in which the many-body wave function, under pairwise exchange of the particle coordinates, picks up a phase θ, which can take any value between 0 (bosons) and π (fermions). Since a phase factor is only a one-dimensional representation of the braid group in two dimensions (2D), the statistics is still Abelian. On the other hand, if the many-body ground-state wave function happens to be a linear combination of states from a degenerate subspace, a pairwise exchange of the particles can unitarily *rotate* the wave function in the ground-state subspace. In this case, the effect of exchanging the particle positions is an operation on the wave-function vector by a unitary matrix representing this rotation. Consequently, the statistics is non-Abelian,[4,5] and the corresponding system is a non-Abelian quantum system. It has been proposed that such systems, if the ground-state subspace is concurrently protected by an energy gap, can be used as a fault-tolerant platform for topological quantum computation (TQC).[4–6]

One important class of non-Abelian quantum systems, sometimes referred to as the Ising topological class,[4] is characterized by quasiparticle excitations called Majorana fermions, which involve no energy cost (when the mutual separation among the excitations is large). The second quantized operators, γ_i, corresponding to these zero-energy excitations are self-Hermitian, $\gamma_i^\dagger = \gamma_i$, which is in striking contrast to ordinary fermionic (or bosonic) operators for which $c_i \neq c_i^\dagger$.

 ©2010 The American Physical Society

However, since γ_i and γ_j anticommute when $i \neq j$, they retain some properties of ordinary fermion operators as well. The Majorana fermions, which are actually more like half fermions, were envisioned by Majorana[7] in 1935 as fundamental constituents of nature (e.g., neutrinos are thought to be Majorana, rather than Dirac, fermions). Majorana modes are intriguing[8] because each Majorana particle is its own antiparticle unlike Dirac fermions where electrons and positrons (or holes) are distinct. Although the emergence of Majorana excitations, which are effectively fractionalized objects (anyons) obeying non-Abelian anyonic statistics, in solid-state systems is by itself an extraordinary phenomenon, a great deal of attention has also been focused on them because of the possibility of carrying out fault tolerant TQC in two-dimensional systems using these Majorana particles. TQC, in contrast to ordinary quantum computation, would not require any quantum error correction since the Majorana excitations are immune to local noise by virtue of their nonlocal topological nature.[4,9] The direct experimental observation of Majorana modes in solid-state systems would therefore be a remarkable breakthrough both from the perspective of fundamental physics of fractional statistics in nature and the technological perspective of building a working quantum computer. It is therefore not surprising that there has been recent resurgence of immense interest for the experimental realization (and detection) of Majorana fermions in solid-state systems. Recently, some exotic ordered states in condensed-matter systems, such as the Pfaffian states in fractional quantum-Hall (FQH) systems,[10–17] p-wave superconductors (SCs)/superfluids,[12,18–31] theoretical models that can be potentially simulated in cold atom optical lattice systems,[32–36] as well as the surface state of a topological insulator (TI) or related systems[37–49] have been discussed as systems which can support Majorana fermions as the lowest energy excitations. In the context of optical systems, it has also been proposed that a 2D p_x+ip_y superfluid can be realized using only s-wave Feshbach resonance modified by the topological Berry phases arising from artificially generated spin-orbit coupling.[50] In the context of optically generated s-wave superfluid systems, a similar topological phase has also been found by considering an artificial "vortexlike" excitation in the spin-orbit coupling parameter in the presence of a magnetic field.[51]

It has been shown recently[52] that even a regular semiconducting film with a sizable Rashba-type spin-orbit coupling, such as InGaAs thin films, can host, under suitable conditions, Majorana fermions as low-energy excitations. Since the basic effects behind the emergence of the Majorana fermion excitations—spin-orbit coupling, s-wave superconductivity, and Zeeman splitting—are physically well understood and experimentally known to occur in many solid-state materials, the proposed semiconductor heterostructure[52] is possibly one of the simplest condensed-matter systems supporting Majorana quasiparticles and non-Abelian quantum order. By an analysis of the real-space Bogoliubov-de Gennes (BdG) equations for a vortex in the semiconductor thin film, in which s-wave superconductivity and a Zeeman splitting are proximity induced [Fig. 1(a)], it has been shown that the lowest energy quasiparticle excitation in the vortex core is a zero-energy Majorana fermion mode. This real-space analysis has also been supported by a momentum-space analysis in the form of an index theorem[53] analogous to such a treatment in the context of one-dimensional Dirac theory.[54,55] Here a comment about the various means to induce a Zeeman splitting in the semiconductor thin film is in order. Note that when the spin-orbit coupling is of the Rashba type, we require a Zeeman splitting which is perpendicular to the plane of the film (Zeeman splitting parallel to the film does not produce a gap in the one-electron band structure, a firm requirement of our non-Abelian state).[52,53] Inducing such a splitting by applying a strong perpendicular magnetic field is not convenient because the magnetic field will give rise to unwanted order parameter defects such as vortices. It is for this reason that we propose to induce the Zeeman splitting by the exchange proximity effect of an adjacent magnetic insulator (MI) (we ignore the small coupling of the spins in the semiconductor with the actual magnetic field of the magnetic insulator). More recently, it has been shown that, when the spin-orbit coupling also has a component which is of the Dresselhaus type, the appropriate Zeeman splitting can also be induced by applying an in-plane magnetic field.[56] The Majorana mode is separated by a finite energy gap (so-called minigap) from the other conventional fermionic excited states in the vortex core. Thus, for a collection of well-separated vortices, the resulting degenerate ground-state subspace is protected from the environment by the minigap. This enables the potential use of the semiconductor heterostructure in Fig. 1(a) in TQC.

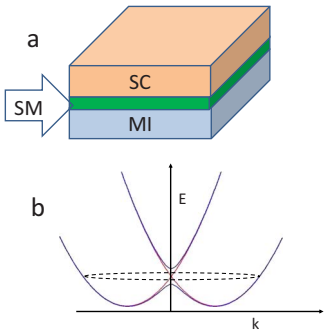

FIG. 1. (Color online) (a) The proposed heterostructure of a semiconductor (SM) sandwiched between an s-wave SC and a magnetic insulator (MI). In this geometry, the semiconducting film can support non-Abelian topological order. (b) Single-particle band structure in the semiconducting film with and without the Zeeman splitting induced by the MI. Without the Zeeman splitting, the two spin-orbit shifted bands touch at $k_x=k_y=|k|=0$ (red lines). Then, for any value of the chemical potential, the system has two Fermi surfaces. With a finite Zeeman splitting, the bands have an energy gap near $k_x=k_y=|k|=0$ (blue lines). If the chemical potential lies in the gap, the system just has one Fermi surface (indicated by the dotted circle).

One of the main goals of the present paper is to provide the important mathematical details relevant to our solutions of the BdG equations in the semiconductor heterostructure. These mathematical details, which were left out in Ref. 52, are given in Secs. II and III below. It is important to note that, unlike the case of the surface of a three-dimensional (3D) strong topological insulator adjacent to an s-wave

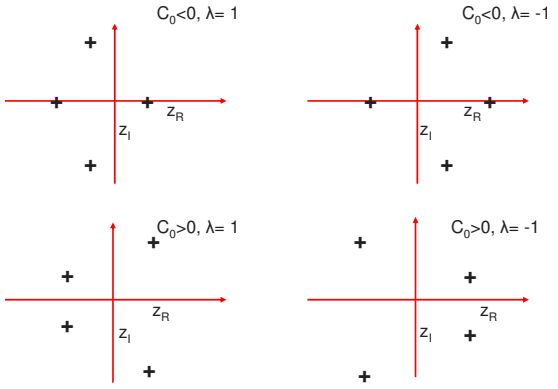

FIG. 2. (Color online) Complex roots $z=z_R+\imath z_I$ of the characteristic equation, Eq. (25), shown in the complex plane. Only solutions with $\mathrm{Re}(z)=z_R>0$ are physically acceptable. In the non-Abelian phase $[C_0=(\Delta^2+\mu^2-V_Z^2)<0]$, three roots with positive real parts and one root with negative real part for $\lambda=-1$ while there are only two roots on either side of the imaginary axis for $C_0>0$ for $\lambda=-1$. The roots in the $\lambda=1$ channel are the negative of the roots in the $\lambda=1$ channel.

superconductor,[37] the BdG equations in the spin-orbit-coupled semiconductor are not exactly solvable. We therefore only show that, in a specified region of the parameter space, a single nondegenerate solution of the BdG equations, which is spatially localized around the vortex core, is allowed. We also show that the second quantized operator corresponding to such a solution is indeed a Majorana fermion operator. (In a subsequent section (Sec. VI) we confirm the existence of such zero-energy Majorana fermion states localized at the vortex cores by a full numerical solution of the BdG equations set up on a sphere.) In the next few sections (Secs. IV–IX) we provide a comprehensive discussion of the interesting physics of non-Abelian topological order arising via the complex interplay of spin-orbit coupling, Zeeman splitting, and *s*-wave superconductivity externally induced in a host system. We also deduce the parameter space needed for the establishment of the non-Abelian order, as well as the associated topological quantum phase transition (TQPT) accessed by tuning the system in or out of this parameter space. In Sec. X we study the superconducting and magnetic proximity effects in the host semiconductor thin film by a microscopic model tight-binding calculation. In the last part of the paper (Sec. XI), we consider a one-dimensional version of our proposed structure—a semiconducting nanowire with proximity-induced *s*-wave superconductivity and a Zeeman splitting. We emphasize that the Zeeman splitting can now be induced by a magnetic field parallel to the length of the wire because such a field does produce a gap in the one-electron band structure without producing unwanted excitations in the adjacent superconductor. This obviates the need for a nearby magnetic insulator. For the Zeeman splitting above a critical value, the wire is in a non-Abelian topological phase with zero-energy Majorana excitations at the ends. We propose a scanning tunneling experiment from the ends of the semiconducting nanowire as possibly the most realistic experiment proposed so far to detect a Majorana fermion state in a condensed-matter system.

We use the terminology Majorana particle or Majorana fermion or Majorana state or Majorana excitation or Majorana mode interchangeably in this paper, all of them meaning precisely the same entity, namely, the nondegenerate zero-energy eigenstate (i.e., a solution of the BdG equations) at the vortex core of a spinless chiral *p*-wave or other such topological superconductor. We emphasize that this object obeys the non-Abelian braiding statistics rather than ordinary fermionic statistics, and the Majorana particle is its own antiparticle in contrast to the ordinary Dirac fermions where electrons and holes (positrons) are distinct particle-hole conjugates of each other. A part of the results presented in this paper—approximate solutions of the BdG equations in the semiconductor heterostructure—has been published elsewhere.[52] In Secs. II and III we provide all the mathematical details relevant to the solutions of the BdG equation which were left out in Ref. 52. Most of the results contained in the subsequent sections are new. Some additional mathematical details related to the solution of the BdG equations are relegated to the Appendix.

II. HAMILTONIAN

The single-particle effective Hamiltonian H_0 for the conduction band of a spin-orbit-coupled semiconductor in contact with a magnetic insulator is given by (we set $\hbar=1$ henceforth)

$$H_0=\frac{p^2}{2m^*}-\mu+V_z\sigma_z+\alpha(\vec{\sigma}\times\vec{p})\cdot\hat{z}. \tag{1}$$

Here, m^*, V_z, and μ are the conduction-band effective mass of an electron, effective Zeeman coupling induced by proximity to a magnetic insulator (we neglect the direct coupling of the electrons with the magnetic field from the magnetic insulator), and chemical potential, respectively. The coefficient α describes the strength of the Rashba spin-orbit coupling and σ_α are the Pauli matrices.

The proximity-induced superconductivity in the semiconductor can be described by the Hamiltonian,

$$\hat{H}_p=\int d\mathbf{r}\{\Delta(\mathbf{r})\hat{c}_\uparrow^\dagger(\mathbf{r})\hat{c}_\downarrow^\dagger(\mathbf{r})+\mathrm{H.c}\}, \tag{2}$$

where $\hat{c}_\sigma^\dagger(\mathbf{r})$ are the creation operators for electrons with spin σ and $\Delta(\mathbf{r})$ is the proximity-induced gap. The pairing term $\hat{H}_p$ and the noninteracting part H_0 can be combined to obtain the BCS mean-field Hamiltonian $H_{\mathrm{BCS}}=H_0+H_p$. The excitation spectrum of this Hamiltonian is defined in terms of the Bogoliubov quasiparticle operators

$$\hat{\gamma}^\dagger=\int d\mathbf{r}\sum_\sigma u_\sigma(\mathbf{r})\hat{c}_\sigma^\dagger(\mathbf{r})+v_\sigma(\mathbf{r})\hat{c}_\sigma(\mathbf{r}), \tag{3}$$

which satisfy

$$[\hat{H}_{\mathrm{BCS}},\hat{\gamma}^\dagger]=E\hat{\gamma}^\dagger. \tag{4}$$

Such a quasiparticle operator $\hat{\gamma}$ can be used to construct excited states $\hat{\gamma}^\dagger|\Psi_0\rangle$ with energy $E+E_0$ from the ground state $|\Psi_0\rangle$ with energy E_0. The ground state $|\Psi_0\rangle$ is defined as the

lowest energy state of the BCS Hamiltonian satisfying $\hat{\gamma}|\Psi_0\rangle=0$. The equation for the quasiparticle operator, Eq. (4), can be rewritten as the BdG equations in the Nambu basis,

$$\begin{pmatrix} H_0 & \Delta(\mathbf{r}) \\ \Delta^*(\mathbf{r}) & -\sigma_y H_0^* \sigma_y \end{pmatrix} \Psi(\mathbf{r}) = E\Psi(\mathbf{r}). \tag{5}$$

Here, $\Psi(\mathbf{r})$ is the wave function in the Nambu spinor basis, $\Psi(\mathbf{r})=[u_\uparrow(\mathbf{r}),u_\downarrow(\mathbf{r}),v_\downarrow(\mathbf{r}),-v_\uparrow(\mathbf{r})]^T$. Introducing the Pauli matrices τ_α in the Nambu space the Hamiltonian on the left-hand side in Eq. (5) can be written as

$$H_{\mathrm{BdG}} = \left[\frac{p^2}{2m^*} - \mu + V_z\sigma_z + \alpha(\vec{\sigma}\times\vec{p})\cdot\hat{z}\right]\tau_z + [\Delta(\boldsymbol{r})\tau_+ + \mathrm{H.c.}], \tag{6}$$

where $\tau_+=\tau_-^\dagger=\frac{\tau_x+\imath\tau_y}{2}$.

III. BdG EQUATIONS FOR A VORTEX

The single-particle Hamiltonian H_0 can be written in polar coordinates as

$$\begin{aligned} H_0 &= \eta p^2 - \mu + V_z\sigma_z + \alpha(\sigma\times p)\cdot\hat{z} \\ &= -\eta\nabla^2 - \mu + V_z\sigma_z + \imath\frac{\alpha}{2}(\sigma_+p_- - \sigma_-p_+), \end{aligned} \tag{7}$$

where $\eta=\frac{\hbar^2}{2m^*}$, $\sigma_+=\sigma_-^\dagger=\sigma_x+\imath\sigma_y$, $p_+=p_x+\imath p_y=e^{\imath\theta}(-\imath\partial_r+\frac{1}{r}\partial_\theta)$, and $p_-=p_x-\imath p_y=e^{-\imath\theta}(-\imath\partial_r-\frac{1}{r}\partial_\theta)$. The full BdG Hamiltonian for an n-fold vortex can be written conveniently in the Nambu space as

$$\begin{aligned} H_{\mathrm{BdG}} &= (-\eta\nabla^2-\mu)\tau_z + V_z\sigma_z + \imath\frac{\alpha}{2}(\sigma_+p_- - \sigma_-p_+)\tau_z + \Delta(r) \\ &\times[\cos(n\theta)\tau_x + \sin(n\theta)\tau_y]. \end{aligned} \tag{8}$$

In order to diagonalize the above Hamiltonian it is convenient to note that the BdG Hamiltonian has a combined spin-orbit-pseudospin rotational symmetry. This symmetry can be expressed compactly by noting that H_{BdG} commutes with the operator

$$J_z = L_z + \frac{1}{2}(\sigma_z - n\tau_z). \tag{9}$$

Therefore, the eigenspinors of the BdG Hamiltonian can be taken to be J_z eigenstates with eigenvalue $J_z=m_J$ of the form

$$\begin{aligned} \Psi_{m_J}(r,\theta) &= e^{\imath L_z\theta}\Psi_{m_J}(r) \\ &= e^{\imath(m_J-\sigma_z/2+n\tau_z/2)\theta}\Psi_{m_J}(r) \\ &= \begin{pmatrix} u_{\uparrow,m_J}(r)e^{\imath(m_J+n-1/2)\theta} \\ u_{\downarrow,m_J}(r)e^{\imath(m_J+n+1/2)\theta} \\ v_{\downarrow,m_J}(r)e^{\imath(m_J-n+1/2)\theta} \\ -v_{\uparrow,m_J}(r)e^{\imath(m_J-n-1/2)\theta} \end{pmatrix}. \end{aligned} \tag{10}$$

The above equation can be used to eliminate the angular degree of freedom θ from the BdG equations as follows:

$$H_{\mathrm{BdG}}\Psi_{m_J}(r,\theta) = E_{m_J}\Psi_{m_J}(r,\theta), \tag{11}$$

$$\tilde{H}_{\mathrm{BdG},m_J}\Psi_{m_J}(r) = E_{m_J}\Psi_{m_J}(r). \tag{12}$$

Here $\tilde{H}_{\mathrm{BdG},m_J}=e^{-\imath(m_J-\sigma_z/2+n\tau_z/2)\theta}H_{\mathrm{BdG}}e^{\imath(m_J-\sigma_z/2+n\tau_z/2)\theta}$ is θ independent. More specifically

$$\begin{aligned} \tilde{H}_{\mathrm{BdG},m_J} &= -\left\{\eta\left[\partial_r^2 + \frac{1}{r}\partial_r + \frac{(2m_J-\sigma_z+n\tau_z)^2}{4r^2}\right] + \mu\right\}\tau_z \\ &+ V_z\sigma_z - \frac{\imath\alpha}{2}\{\sigma_+ - \sigma_-\}\tau_z\partial_r - \imath\frac{\alpha}{2r}\left\{\sigma_+\frac{2m_J+n\tau_z+1}{2}\right. \\ &\left. + \sigma_-\frac{2m_J+n\tau_z-1}{2}\right\}\tau_z + \Delta(r)\tau_x. \end{aligned} \tag{13}$$

Under the action of the particle-hole transformation operator, $\Xi=\sigma_y\tau_yK$, the m_J spinor eigenstate with energy E transforms into a $-m_J$ eigenstate with energy $-E$ because

$$\Xi e^{\imath(m_J-\sigma_z/2+n\tau_z/2)\theta}\Psi_{m_J}(r) = e^{\imath(-m_J-\sigma_z/2+n\tau_z/2)\theta}\Xi\Psi_{m_J}(r).$$

Therefore, a necessary condition for a nondegenerate, $E=0$, Majorana state solution is that $m_J=0$. From here onward we will write $\tilde{H}_{\mathrm{BdG},m_J=0}=\tilde{H}_{\mathrm{BdG}}$ and $\Psi_{m_J=0}(r)=\Psi(r)$. Single valuedness of the spinor wave functions in Eq. (10) requires that $(n-1)/2$ must be an integer. Therefore, only odd vortices can have nondegenerate Majorana eigenstates. From here onward, for the simplicity of discussion, we will consider only zero-energy solutions at the cores of single-flux-quantum vortices ($n=1$).

The BdG matrix $\tilde{H}_{\mathrm{BdG}}$ may be reduced to a real Hamiltonian by applying the σ_z rotation $U=e^{\imath\sigma_z\pi/4}$ as $\tilde{H}_{\mathrm{BdG}} \rightarrow U^\dagger\tilde{H}_{\mathrm{BdG}}U$. The solutions of the resulting $E=0$ BdG equation $\tilde{H}_{\mathrm{BdG}}\Psi(r)=0$ must come in complex conjugate pairs $\Psi(r)$ and $\Psi^*(r)$. Therefore the solutions $\Psi(r)$ can be required to be real without loss of generality. For such real solutions, it follows from the particle-hole symmetry of the BdG equations that $\sigma_y\tau_y\Psi(r)$ is also a solution. Thus, any nondegenerate $E=0$ solution must be real and satisfy the property $\sigma_y\tau_y\Psi(r)=\lambda\Psi(r)$. Moreover, because $(\sigma_y\tau_y)^2=1$, the possible values of λ are $\lambda=\pm1$.

Using the relation $\tau_x=\imath\lambda\sigma_y\tau_z$, which follows from $\sigma_y\tau_y=\lambda$, the BdG Hamiltonian for a given value of λ is of the form

$$\begin{aligned} \tilde{H}_{\mathrm{BdG}} &= -\left\{\eta\left[\partial_r^2 + \frac{1}{r}\partial_r + \frac{(-\sigma_z+\tau_z)^2}{4r^2}\right] + \mu\right\}\tau_z + V_z\sigma_z - \frac{\alpha}{2}\{\sigma_+ \\ &+ \sigma_-\}\tau_z\partial_r - \frac{\alpha}{2r}\left\{\sigma_+\frac{\tau_z+1}{2} + \sigma_-\frac{\tau_z-1}{2}\right\}\tau_z + \imath\lambda\sigma_y\tau_z\Delta(r). \end{aligned} \tag{14}$$

The Hamiltonian in this limit does not couple the $\tau_z=\pm1$ sectors (electron and hole). This allows one to write the BdG differential equation in terms of only the electron sector ($\tau_z=+1$) of the spinor $\Psi_0(r)=[u_\uparrow(r),u_\downarrow(r)]^T$. The corresponding reduced BdG equations for a single vortex ($n=1$) take the form of a 2×2 matrix differential equation,

$$\begin{pmatrix} -\eta\left(\partial_r^2+\frac{1}{r}\partial_r\right)+V_z-\mu & \lambda\Delta(r)+\alpha\left(\partial_r+\frac{1}{r}\right) \\ -\lambda\Delta(r)-\alpha\partial_r & -\eta\left(\partial_r^2+\frac{1}{r}\partial_r-\frac{1}{r^2}\right)-V_z-\mu \end{pmatrix}\Psi_0(r)=0. \tag{15}$$

The hole part of the spinor is not independent and is constrained by the value of λ such that $v_\uparrow(r)=\lambda u_\uparrow(r)$ and $v_\downarrow(r)=\lambda u_\downarrow(r)$ and the Majorana spinor has the form $\Psi(\boldsymbol{r})=[\Psi_0(\boldsymbol{r}),\iota\sigma_y\Psi_0(\boldsymbol{r})^*]^T$.

We now approximate the radial dependence of $\Delta(r)$ by $\Delta(r)=0$ for $r<R$ and $\Delta(r)=\Delta$ for $r\geq R$, where R is on the order of the radius of a vortex core. In view of the topological stability of the putative Majorana zero-energy solution to local changes in the Hamiltonian,[12] such an approximation can be made without any loss of generality.

A. Solution inside the vortex core

Inside the vortex core ($r<R$), which is the nonsuperconducting region [$\Delta(r)=0$], it is possible to construct explicit analytic solutions $\Psi(r,z)$ to these equations in terms of the Bessel functions $J_0(z)$ and $J_1(z)$ as

$$\Psi(r,z)=\begin{pmatrix} u_\uparrow J_0(zr) \\ u_\downarrow J_1(zr) \end{pmatrix}. \tag{16}$$

By substituting Eq. (16) into Eq. (15) we find that $(u_\uparrow,u_\downarrow)$ and z satisfy

$$\begin{pmatrix} \eta\left(-\partial_r^2-\frac{1}{r}\partial_r\right)+V_z-\mu & \alpha\left(\partial_r+\frac{1}{r}\right) \\ -\alpha(\partial_r) & \eta\left(-\partial_r^2-\frac{1}{r}\partial_r+\frac{1}{r^2}\right)-V_z-\mu \end{pmatrix} \times\begin{pmatrix} u_\uparrow J_0(zr) \\ u_\downarrow J_1(zr) \end{pmatrix} = \begin{pmatrix} (-\eta z^2+V_z-\mu)u_\uparrow J_0(zr)+z\alpha u_\downarrow J_0(zr) \\ z\alpha u_\uparrow J_1(zr)+(-\eta z^2-V_z-\mu)u_\downarrow J_1(zr) \end{pmatrix}=0, \tag{17}$$

which implies

$$\begin{pmatrix} -\eta z^2+V_z-\mu & z\alpha \\ \alpha z & -\eta z^2-V_z-\mu \end{pmatrix}\begin{pmatrix} u_\uparrow \\ u_\downarrow \end{pmatrix}=0. \tag{18}$$

Existence of solutions in terms of $(u_\uparrow,u_\downarrow)^T$ requires that z satisfies the characteristic equation of the matrix in Eq. (18), which is given by

$$(\eta z^2-\mu)^2-V_z^2-z^2\alpha^2=0. \tag{19}$$

This is a quadratic equation in z^2 with real roots. Therefore, the solutions for z are either purely real or purely imaginary and come in pairs with opposite signs. A real root $z=k$ of this equation corresponds to a crossing of some band at the Fermi level. For purely real roots z, only the solution $\Psi(r,z)$ corresponding to positive z is normalizable at the origin and therefore physically acceptable. On the other hand, the purely imaginary roots $z=\pm\iota k$ lead to a single real solution $\Psi(r,\iota k)=\Psi(r,-\iota k)$. Thus we can see that in general there are two linearly independent solutions. If all four solutions of z are real then these correspond to the two Fermi surfaces obtained from the intersection of the bands with the Fermi level. If only one pair of solutions is real then the imaginary pair corresponds to a decaying state.

The BdG equations describing the proximity-induced superconductivity at a TI/SC interface[37] follow from the BdG equations for the present system, Eq. (15), by taking $\eta=0$. In this case the matrix equation reduces to

$$\begin{pmatrix} V_z-\mu & z\alpha \\ \alpha z & -V_z-\mu \end{pmatrix}\begin{pmatrix} u_\uparrow \\ u_\downarrow \end{pmatrix}=0. \tag{20}$$

This equation only has one pair of real solutions $z=\pm\sqrt{\mu^2-V_z^2}/\alpha$ and therefore has only one linearly independent solution in the core of the vortex.

B. Solution outside the vortex core

The solution outside the vortex does not have a simple analytic form as the solution inside. Motivated by the large r asymptotic expansion for Bessel functions, for $r>R$ we can consider a series expansion of the form

$$\begin{pmatrix} u_\uparrow(r) \\ u_\downarrow(r) \end{pmatrix}=\frac{e^{-zr}}{r^{1/2}}\begin{pmatrix} \rho_\uparrow(1/r) \\ \rho_\downarrow(1/r) \end{pmatrix}, \tag{21}$$

where $\rho(x)$ are analytic power series in x. We expect to be able to close such a series of equations since the matrix in Eq. (15) only has derivatives and powers of $1/r$,

$$\begin{pmatrix} \eta\left(-\partial_r^2-\frac{1}{r}\partial_r\right)+V_z-\mu & \lambda\Delta+\alpha\left(\partial_r+\frac{1}{r}\right) \\ -\lambda\Delta-\alpha(\partial_r) & \eta\left(-\partial_r^2-\frac{1}{r}\partial_r+\frac{1}{r^2}\right)-V_z-\mu \end{pmatrix}\frac{e^{-zr}}{r^{1/2}}\begin{pmatrix} \rho_\uparrow(1/r) \\ \rho_\downarrow(1/r) \end{pmatrix}=0, \tag{22}$$

$$\begin{pmatrix} \eta\left(-\partial_r^2-\frac{1}{4r^2}+2z\partial_r-z^2\right)+V_z-\mu & \lambda\Delta+\alpha\left(\partial_r+\frac{1}{2r}-z\right) \\ -\lambda\Delta-\alpha\left(\partial_r-\frac{1}{2r}-z\right) & \eta\left(-\partial_r^2+\frac{3}{4r^2}+2z\partial_r-z^2\right)-V_z-\mu \end{pmatrix}\begin{pmatrix}\rho_\uparrow(1/r)\\ \rho_\downarrow(1/r)\end{pmatrix}=0. \tag{23}$$

As shown in the Appendix, the last equation has a simple solution as a power series in $1/r$ which can be determined numerically. Moreover in this power-series expansion we can determine the equation for the zeroth-order term by formally setting $1/r=0$ as below

$$\begin{pmatrix} -\eta z^2+V_z-\mu & \lambda\Delta-z\alpha \\ -\lambda\Delta+z\alpha & -\eta z^2-V_z-\mu \end{pmatrix}\begin{pmatrix}\rho_\uparrow(0)\\ \rho_\downarrow(0)\end{pmatrix}=0. \tag{24}$$

Setting $z=\imath k$ one can see that the matrix appearing in the above equation is related to the one determining the quasiparticle band structure from the BdG equations. Normalizability of the solutions in Eq. (21), require that they be exponentially decaying. This constrains physically acceptable solutions to satisfy the constraint $\mathrm{Re}(z)>0$. The values of z consistent with the above equation are determined by setting

$$\mathrm{Det}\begin{pmatrix} -\eta z^2+V_z-\mu & \lambda\Delta-z\alpha \\ -\lambda\Delta+z\alpha & -\eta z^2-V_z-\mu \end{pmatrix} = (\eta z^2-\mu)^2-V_z^2+(z\alpha\mp\Delta)^2=0. \tag{25}$$

The two families of solution for $\lambda=\pm 1$ are related simply by flipping the sign of z. The sign of the product of the roots z_n of Eq. (25) is given by $S=\mathrm{sgn}[\Pi_n(z_n)]=\mathrm{sgn}(C_0)$, where $C_0=(\mu^2+\Delta^2-V_Z^2)$ is the polynomial evaluated at $z=0$. The parity of the number of normalizable solutions with $\mathrm{Re}(z_n)>0$ is given by $P=\mathrm{sgn}[\Pi_n\mathrm{Re}(z_n)]$. Since Eq. (25) is real, complex roots z_n occur in conjugate pairs. Therefore, complex roots cannot affect the sign of either S or P. It follows that $S=P$.

Therefore, the condition $|V_Z|>\sqrt{\Delta^2+\mu^2}$ implies that there are an odd number of roots with positive real parts. Specifically, as seen in Fig. 2, if $C_0<0$, there are three roots on one side of the imaginary axis and one root on the other side. Similarly for $C_0>0$ we must have two solutions on each side of the imaginary axis. A slightly different version of this argument has previously been presented.[57]

C. Matching boundary conditions at the edge of the vortex core

As discussed before, for $\Delta^2+\mu^2>V_Z^2$, one of the channels labeled by $\pm$ has a solution with three decaying (negative real parts) solutions and one growing solution. Out of these three decaying solutions, one is purely real and negative and the other two are complex conjugate with negative real parts. An observation that can be made by considering Eq. (23) is that if $[\rho_\uparrow(1/r),\rho_\downarrow(1/r)]^T$ corresponds to a value z then $[\rho_\uparrow^*(1/r),\rho_\downarrow^*(1/r)]^T$ corresponds to an eigenvalue z^*. Thus from one pair of complex conjugate decaying eigenvalues we can construct a pair of real solutions

$$\begin{pmatrix}u_{\uparrow,(1,2)}(r)\\ u_{\downarrow,(1,2)}(r)\end{pmatrix}=s_{(1,2)}\left\{e^{-zr}\begin{pmatrix}\rho_\uparrow(1/r)\\ \rho_\downarrow(1/r)\end{pmatrix}\pm e^{-z^*r}\begin{pmatrix}\rho_\uparrow^*(1/r)\\ \rho_\downarrow^*(1/r)\end{pmatrix}\right\}, \tag{26}$$

where $s_1=1$ and $s_2=\imath$ with the solution 1 corresponding to + and 2 to −.

The nondegenerate real eigenvalue already corresponds to a real eigenvector

$$\begin{pmatrix}u_{\uparrow,3}(r)\\ u_{\downarrow,3}(r)\end{pmatrix}=e^{-zr}\begin{pmatrix}\rho_\uparrow(1/r)\\ \rho_\downarrow(1/r)\end{pmatrix}. \tag{27}$$

On the other hand, for $r<R$ we expect a two-parameter family with the general solution given by

$$\begin{pmatrix}v_\uparrow(r)\\ v_\downarrow(r)\end{pmatrix}=a_4\begin{pmatrix}u_{\uparrow,4}(r)\\ u_{\downarrow,4}(r)\end{pmatrix}+a_5\begin{pmatrix}u_{\uparrow,5}(r)\\ u_{\downarrow,5}(r)\end{pmatrix}. \tag{28}$$

Matching the gradient and the wave function at $r=R$ we get

$$\begin{pmatrix}v_\uparrow(R)\\ v_\downarrow(R)\\ \partial_r v_\uparrow(R)\\ \partial_r v_\downarrow(R)\end{pmatrix}=a_4\begin{pmatrix}u_{\uparrow,4}(R)\\ u_{\downarrow,4}(R)\\ \partial_r u_{\uparrow,4}(R)\\ \partial_r u_{\downarrow,4}(R)\end{pmatrix}+a_5\begin{pmatrix}u_{\uparrow,5}(R)\\ u_{\downarrow,5}(R)\\ \partial_r u_{\uparrow,5}(R)\\ \partial_r u_{\downarrow,5}(R)\end{pmatrix}=\sum_{j=1}^{3}a_j\begin{pmatrix}u_{\uparrow,j}(R)\\ u_{\downarrow,j}(R)\\ \partial_r u_{\uparrow,j}(R)\\ \partial_r u_{\downarrow,j}(R)\end{pmatrix}. \tag{29}$$

Together with the normalization constraint on the global wave function, this leads to five equations in five variables, which leads to a unique solution for the Majorana mode in the case $C_0<0$. However, for the other case with $C_0>0$, there are only two decaying modes outside the vortex core. The existence of a Majorana mode would then require us to satisfy five equations with four variables. Such a problem in general is over constrained and no Majorana solutions exist in this case.

IV. MAJORANA SOLUTION FOR VORTEX IN THE SPIN-ORBIT COUPLING

For a planar system, the Rashba spin-orbit term $\alpha(\boldsymbol{\sigma}\times\boldsymbol{p})\cdot\hat{z}$ in the Hamiltonian we considered can also be written as $\alpha\boldsymbol{\sigma}\cdot\boldsymbol{p}$. These two terms are simply related to each other by a σ_z spin rotation and a more general Rashba-type spin-orbit term can be written as

$$H_{SO} = \alpha[\cos\,\zeta(\boldsymbol{\sigma}\times\boldsymbol{p})\cdot\hat{z} + \sin\,\zeta\boldsymbol{\sigma}\cdot\boldsymbol{p}]. \tag{30}$$

A recent proposal[51] has considered a defect in such a spin-orbit coupling where the angle of the spin-orbit ζ varies in space to form a vortex $[\zeta(\theta)=\theta]$. The full BdG Hamiltonian for such a vortex can be written in Nambu space as

$$H_{\mathrm{BdG}} = (-\eta\nabla^2-\mu)\tau_z + V_z\sigma_z + \frac{1}{4}(\sigma_+\{\alpha(r)e^{\iota\theta},p_-\} + \sigma_-\{\alpha(r)e^{-\iota\theta},p_+\})\tau_z + \Delta\tau_x, \tag{31}$$

where the anticommutation must be introduced in the spin-orbit term to preserve Hermiticity.

Substituting the circular-polar form for the derivatives we note that the Hamiltonian becomes

$$\tilde{H}_{\mathrm{BdG}} = -\left[\eta\left(\partial_r^2+\frac{1}{r}\partial_r-\frac{\partial_\theta^2}{4r^2}\right)+\mu\right]\tau_z + V_z\sigma_z - \frac{\iota}{2}\left\{\sigma_+\left\{[\partial_r,\alpha(r)]+\frac{\alpha(r)}{r}\{e^{-\iota\theta},e^{\iota\theta}\partial_\theta\}\right\}+\mathrm{H.c.}\right\}+\Delta\tau_x, \tag{32}$$

which in turn simplifies to a θ-independent form

$$\tilde{H}_{\mathrm{BdG}} = -\left[\eta\left(\partial_r^2+\frac{1}{r}\partial_r-\frac{\partial_\theta^2}{4r^2}\right)+\mu\right]\tau_z + V_z\sigma_z - \frac{1}{2}\left\{\sigma_+\left\{[\alpha(r)\partial_r+\alpha'(r)]-\frac{\iota\alpha(r)}{r}\{\partial_\theta+\iota\}\right\}+\mathrm{H.c.}\right\}+\Delta\tau_x. \tag{33}$$

Therefore, $J_z=L_z$ commutes with the above Hamiltonian and the spinor form is

$$\psi_{m_J}(r,\theta) = e^{\iota L_z\theta}\psi_{m_J}(r) = e^{\iota m_J\theta}\psi_{m_J}(r) = e^{\iota m_J\theta}\begin{pmatrix} u_{\uparrow,m_J}(r)\\ u_{\downarrow,m_J}(r)\\ v_{\downarrow,m_J}(r)\\ -v_{\uparrow,m_J}(r)\end{pmatrix}. \tag{34}$$

As before only the $m_J=0$ channel can lead to a nondegenerate Majorana solution and the BdG equation in this channel is given by

$$\tilde{H}_{\mathrm{BdG}} = -\left[\eta\left(\partial_r^2+\frac{1}{r}\partial_r\right)+\mu\right]\tau_z + V_z\sigma_z - \frac{1}{2}\left\{\sigma_+\left\{[\alpha(r)\partial_r+\alpha'(r)]+\frac{\alpha(r)}{r}\right\}+\mathrm{H.c.}\right\}+\Delta\tau_x. \tag{35}$$

Since the above BdG equation is real, it can be reduced to a 2×2 matrix differential equation,

$$\begin{pmatrix} -\eta\left(\partial_r^2+\frac{1}{r}\partial_r\right)+V_z-\mu & \lambda\Delta+\alpha(r)\partial_r+\alpha'(r)+\frac{\alpha(r)}{r}\\ -\lambda\Delta+\alpha(r)\partial_r+\alpha'(r)+\frac{\alpha(r)}{r} & -\eta\left(\partial_r^2+\frac{1}{r}\partial_r\right)-V_z-\mu\end{pmatrix}\Psi_0(r)=0. \tag{36}$$

As before, considering a step-function vortex profile $\alpha(r)=0$ for $r<R$ and $\alpha(r)=\alpha$ for $r>R$, one notices that the reduced BdG equation outside the spin-orbit vortex core resembles the reduced BdG equation in the same region for a regular vortex in the large r limit [Eq. (15) with $\Delta(r)=\Delta$]. Inside the vortex core $\alpha(r)=0$, and the BdG equations, as before, are analytically solvable via Bessel functions as below

$$\begin{pmatrix} \eta\left(-\partial_r^2-\frac{1}{r}\partial_r\right)+V_z-\mu & \lambda\Delta\\ -\lambda\Delta & \eta\left(-\partial_r^2-\frac{1}{r}\partial_r\right)-V_z-\mu\end{pmatrix}\times\begin{pmatrix} u_\uparrow J_0(zr)\\ u_\downarrow J_0(zr)\end{pmatrix}=0, \tag{37}$$

where

$$\begin{pmatrix} -\eta z^2+V_z-\mu & \lambda\Delta\\ -\lambda\Delta & -\eta z^2-V_z-\mu\end{pmatrix}\begin{pmatrix} u_\uparrow\\ u_\downarrow\end{pmatrix}=0. \tag{38}$$

As before, this leads to two solutions inside and three solutions outside the vortex core, with five constraints at the interface. This leads to a single nondegenerate Majorana solution at the interface.

The previous calculation of the wave function of the system discussed in this section in Ref. 51 yielded the result $\psi_0(r)\propto e^{-(V_Z-\Delta)r/\alpha}$ for the asymptotic $(r\to\infty)$ behavior of the zero-energy wave function. For small $\Delta<V_Z$, and $\mu=0$ we find that the asymptotic zero-energy wave function behaves as $\psi_0(r)\propto e^{-\Delta r/\alpha}\frac{e^{-\iota\alpha r/\eta}}{\sqrt{r}}$. Further that the previous result $\psi_0(r)\propto e^{-(V_Z-\Delta)r/\alpha}$,[51] is valid only in the limit $V_Z-\Delta\ll\Delta$, which excludes the limit of small Δ. Our result, $\psi_0(r)\propto e^{-\Delta r/\alpha}\frac{e^{-\iota\alpha r/\eta}}{\sqrt{r}}$, can be understood from the physically reasonable requirement that the Majorana fermion becomes more delocalized in the limit of weak superconductivity (small Δ). According

to our result for small Δ, the decay length of the zero-energy wave function diverges in the limit of vanishingly weak superconductivity ($\Delta \to 0$) and the Majorana mode disappears by delocalizing over the entire system.

V. MAJORANA SOLUTION ON THE SURFACE OF A TOPOLOGICAL INSULATOR

Now we apply a similar argument to the vortex in proximity-induced *s*-wave superconductivity on a TI surface[37] which is obtained from our Rashba model by setting $\eta=0$. The equation for the allowed values of z in the superconductor for $r>R$ are then

$$\mu^2 - V_z^2 + (z\alpha \mp \Delta)^2 = 0, \tag{39}$$

$$z = \pm(\Delta \pm \imath\sqrt{\mu^2 - V_z^2})/\alpha. \tag{40}$$

Therefore, in each of the $\pm$ channels, for small V_z, there are a pair of complex conjugate eigenvalues on the same side of the imaginary axis. For the + channel both the eigenvalues are to the right of the imaginary axis and therefore are acceptable decaying solutions. Thus there are two linearly independent solutions $(u_{\uparrow,1}, u_{\downarrow,1})$ and $(u_{\uparrow,2}, u_{\downarrow,2})$ for $r>R$. From our previous discussion it is now clear that there is only one such solution $(u_{\uparrow,3}, u_{\downarrow,3})$ for $r<R$.

Since the Hamiltonian is linear in the derivative, the boundary conditions only require us to match the wave function $[u_\uparrow(r), u_\downarrow(r)]^T$ at $r=R$ and not the derivative. The boundary conditions that the zero-energy solution must satisfy at $r=R$ are given by

$$\begin{pmatrix} u_\uparrow(R) \\ u_\downarrow(R) \end{pmatrix} = a_3 \begin{pmatrix} u_{\uparrow,3}(R) \\ u_{\downarrow,3}(R) \end{pmatrix} = \sum_{j=1}^{2} a_j \begin{pmatrix} u_{\uparrow,j}(R) \\ u_{\downarrow,j}(R) \end{pmatrix}. \tag{41}$$

Together with the normalization condition for the zero-energy wave function, the above equations provide three constraints for the three variables a_1, a_2, a_3. This yields a unique zero-energy Majorana wave function for a vortex on a TI surface.

VI. NUMERICAL CALCULATION OF THE VORTEX EXCITATION SPECTRUM IN THE SPIN-ORBIT-COUPLED SEMICONDUCTOR

In previous sections we calculate and show the existence of a Majorana mode in a vortex at the interface of an *s*-wave superconductor and a spin-orbit-coupled semiconductor. The most important information missing from these analytical calculations is the excitation gap above the zero-energy Majorana state, the so-called minigap. A proper calculation of this requires a numerical solution of the vortex problem which can be done by considering the system on a sphere with a vortex-antivortex pair[58,59] as shown in the inset of Fig. 3(a).

The BdG Hamiltonian of this problem can be written as

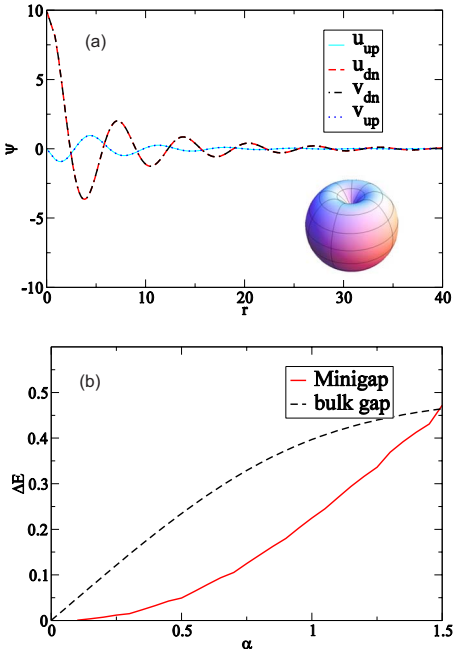

FIG. 3. (Color online) (a) Plots for the individual components of the four-component wave function $\Psi(r)=[u_\uparrow(r), u_\downarrow(r), v_\downarrow(r), -v_\uparrow(r)]^T$ for the zero-energy Majorana state at the north pole. The components of Ψ satisfy $u_\sigma = v_\sigma^*$ confirming the Majorana nature of the wave function. We also show the semiconductor heterostructure on the surface of a sphere with a vortex and an antivortex (with reduced superconducting amplitudes at the vortex cores) situated at the north and the south poles. (b) Numerical results for the vortex minigap ΔE (solid line) and bulk gap (dashed line) plotted against the spin-orbit-coupling strength α on the semiconductor. In these plots we have used $\Delta=0.5$, $\mu=0.0$, and $\eta=1.0$ in the units where $V_z=1$. The spin-orbit-coupling strength $\alpha=0.3$ in (a) and varies for (b). In these units, the size of the vortex core has been taken to be unity.

$$H = \left[\eta \boldsymbol{p}^\dagger \boldsymbol{p} + \frac{\alpha}{2}\{(\sigma \times \hat{R}) \cdot \boldsymbol{p} + \boldsymbol{p}^\dagger \cdot (\sigma \times \hat{R})\} - \mu \right] \tau_z + V_Z \sigma \cdot \hat{R} + \Delta(\mathbf{r})\tau_x, \tag{42}$$

where $\boldsymbol{p} = -\imath[\boldsymbol{\nabla} - \hat{R}(\hat{R}\cdot\boldsymbol{\nabla})]$ is the non-Hermitian gradient operator restricted to the surface of the sphere and $\hat{R}=\frac{r}{r}$. The above Hamiltonian takes a more familiar form in angular coordinates as

$$\begin{aligned} H &= \left[\frac{\eta}{R^2} L^2 - \frac{\alpha}{R} L \cdot \sigma - \mu \right] \tau_z + V_Z \sigma \cdot \hat{R} + \Delta(\theta) \\ &\quad \times \{\cos\phi \tau_x + \sin\phi \tau_y\} \\ &= \left[\frac{\eta}{R^2} L^2 - \frac{\alpha}{R} \left\{ L_z \sigma_z + \frac{1}{2} L_+ \sigma_- + \frac{1}{2} L_- \sigma_+ \right\} - \mu \right] \tau_z \\ &\quad + V_Z \left\{ R_z \sigma_z + \frac{1}{2} R_+ \sigma_- + \frac{1}{2} R_- \sigma_+ \right\} \\ &\quad + \frac{1}{2} \frac{\Delta(\theta)}{\sin\theta} \{R_+ \tau_- + R_- \tau_+\}, \end{aligned} \tag{43}$$

where $R_z=\cos\theta$ and $R_\pm=\sin\theta e^{\pm\imath\phi}$. In these equations $R_-=R_+^\dagger$ and $L_-=L_+^\dagger$. The spectrum of excitations of this system is found by solving the eigenvalue problem

$$H\Psi = E\Psi. \tag{44}$$

Similar to the vortex in the planar geometry, the BdG Hamiltonian has a combined spin-orbit-pseudospin rotational symmetry. This symmetry can be expressed compactly by noting that the Hamiltonian commutes with

$$J_z = L_z + \frac{1}{2}(\sigma_z - \tau_z), \tag{45}$$

where we have used the identity $[R_\pm, L_z] = \pm R_\pm$. The ϕ dependence of the eigenstates with $m_J=m$ can be written as $e^{\imath L_z\phi}\Psi_m(\theta)=e^{\imath(m-(\sigma_z-\tau_z)/2)\phi}\Psi_m(\theta)$. The ϕ-independent part of the eigenstate $\Psi_m(\theta)$ then satisfies a one-dimensional BdG equation $H_m\Psi_m(\theta)=E_m\Psi_m(\theta)$, where

$$H_m = U_m^\dagger(\phi)HU_m(\phi), \tag{46}$$

which can be explicitly checked to be ϕ independent and $U_m(\phi)=e^{\imath[m-(\sigma_z-\tau_z)/2]\phi}$. To solve for the θ-dependent part of $\Psi_m(\theta)$ it is necessary to convert H_m to a discrete matrix by expanding $\Psi_m(\theta)=\Sigma_l c_{l,m}P_l^{(m)}(\cos\theta)$, where $P_l^{(m)}(\cos\theta)$ are the associated Legendre polynomials which are the ϕ-independent parts of the spherical Harmonics. In the associated Legendre polynomial basis the kinetic-energy term L^2 has the simple diagonal form $l(l+1)$. Under the transformation in Eq. (46), the terms $R_{z,\pm}$ in H transform into $P_1^{(0,\pm1)}(\cos\theta)$ in H_m. Therefore, its matrix elements in the associated Legendre polynomial basis can be calculated using the spherical harmonic addition theorem. A similar procedure can be used to calculate the matrix elements of the θ-dependent vortex. For a vortex, we take $\Delta(\theta)=\Delta\tanh R\sin\theta/\xi$, where ξ is taken to be the length scale of the vortex. From symmetry properties it is clear that $\Delta(\theta)/\sin\theta$ is an even polynomial in $\sin\theta$ and can be written in terms of associated Legendre polynomials as

$$\frac{\Delta(\theta)}{\sin\theta} = \sum_l c_{(2l+1)}P^1_{(2l+1)}(\cos\theta), \tag{47}$$

where the associate Legendre polynomial can be written as $P_l^1(\cos\theta)=-\sin\theta P_l'(\cos\theta)$ and $c_l=\frac{(2l+1)}{2l(l+1)}\int_{-1}^1 P_l^1(x)\Delta(x)dx$. As with the R operators, the angular momentum matrix elements can be calculated from the above expansion by using the spherical harmonic addition theorem.

As in the analytic solution for the vortex, the angular momentum index m transforms from $m\to-m$ under the particle-hole transformation Ξ and we expect nondegenerate $E=0$ Majorana solutions of Eq. (44) only in the $m=0$ channel. This is confirmed by our numerical solution of Eq. (44) where we find that only in the topological phase $C_0<0$, are there a pair of states in the $m=0$ angular momentum channel whose eigenvalues approach 0 exponentially with increasing radius R. The nonzero-energy eigenvalue of the Majorana fermion is a result of the presence of two vortices in our calculation with a finite distance between them. The wave function of the $E=0$ eigenvalue of the $m=0$ angular momentum channel, that is localized at the north pole is plotted in Fig. 3(a). The components of the wave function are seen to satisfy $u_\sigma=v_\sigma^*$ confirming the Majorana character of these states. In the figure, the wave functions of the Majorana modes is seen to decay and oscillate away from the north pole. The splitting between the Majorana modes into a pair of exponentially small oscillating eigenvalues is a result of the overlap between the Majorana modes at the two poles.[60]

Aside from the $E=0$ eigenvalue in the $m=0$ angular momentum channel, an isolated vortex confines a set of nonzero eigenvalues in other $m\neq0$ angular momentum channels. Of these, the eigenvalue with the smallest absolute value occurs in the $m=1$ angular momentum channel and has an eigenvalue equal to the so-called minigap of the vortex. As mentioned before, the superconductivity in the non-Abelian superconducting phase is re-entrant with a bulk gap that is proportional to the spin-orbit-coupling strength. As seen from Fig. 3(b) both the bulk and minigap are proportional to the spin-orbit-coupling strength α. For spin-orbit coupling $\alpha\sim1$ and chemical potential $\mu=0$, both the minigap and the bulk gap are of order the induced pairing potential Δ. Therefore for the semiconductor structure where superconductivity is proximity induced, the minigap of a vortex can be tuned to be of order Δ if the chemical potential μ can be tuned to be less than order V_Z, the Zeeman potential applied to the semiconductor. This is different from the conventional case of a regular (not proximity induced) where the chemical potential is of order E_F and the minigap is of order Δ^2/E_F which is much smaller than Δ.

Thus the ability to independently control the chemical potential in the semiconductor heterostructure provides us with a powerful tool that can increase the minigap of the vortex in the semiconductor heterostructure shown in Fig. 1 by orders of magnitude from the values in chiral p-wave superconductors to on the order of 1 K. This leads to the possibility of performing TQC with the Majoranas trapped in vortices in the heterostructure at temperatures which are as large as a fraction of a 1 K.

VII. BULK TOPOLOGICAL QUANTUM PHASE TRANSITION

We found that the Majorana modes exist for a spin-orbit-coupled semiconductor system only in the parameter regime $C_0=(\Delta^2+\mu^2)-V_Z^2<0$. This in turn was related to the parity of the roots in one half of the complex wave-vector plane of solutions outside the vortex core. As pointed out before in the context of Eq. (25), these roots are indeed properties of the reduced bulk superconducting Hamiltonian in the absence of a vortex. We also expect such a connection between the bulk properties and the existence of Majorana modes on general topological grounds.[12]

To show explicitly the connection between the condition for the existence of Majorana modes ($C_0<0$) and the bulk properties, we note that even though the gap in the bulk superconducting state prevents the existence of propagating states at $E=0$, it allows evanescent states. Since the states at $E=0$ are particle-hole symmetric eigenstates Ψ_0 of a real Hamiltonian, we can apply an argument analogous to Eq. (15) to obtain a bulk BdG equation in a λ channel

$$\begin{pmatrix} -\eta\nabla^2 + V_z - \mu & \lambda\Delta + \alpha(\partial_x + \imath\partial_y) \\ -\lambda\Delta - \alpha(\partial_x - \imath\partial_y) & -\eta\nabla^2 - V_z - \mu \end{pmatrix} \Psi_0(x,y) = 0. \tag{48}$$

Considering an evanescent state of the form $\Psi_0(x,y) = e^{-z(x\cos\theta + y\sin\theta)}\Psi_0$ leads to a constraint on z which was previously written as Eq. (25). Therefore, the condition on C_0, which determines whether the phase supports a Majorana solution or not is precisely related to the parity of decaying evanescent modes in a given λ channel in the bulk superconductor at $E=0$.

A change in the parity of the decaying evanescent modes requires an $E=0$ mode to become propagating, which can only exist if the bulk superconductor is gapless. Therefore, a change in the sign of C_0, which determines the topological nature of the phase, must be accompanied by a closing of the bulk spectrum. This is determined by the full BdG Hamiltonian for a state with momentum $k(\cos\theta, \sin\theta)$ and can be written in the Nambu space as

$$H_{\mathrm{BdG}} = (\eta k^2 - \mu)\tau_z + V_z\sigma_z + \frac{\imath\alpha k}{2}(e^{-\imath\theta}\sigma_+ - e^{\imath\theta}\sigma_-)\tau_z + \Delta\tau_x. \tag{49}$$

The spectrum is obtained by considering $\mathrm{Det}(H_{\mathrm{BdG}} - E_k) = 0$ which can be simplified to the equation,

$$E_k^2 = V_z^2 + \Delta^2 + \tilde{\epsilon}^2 + \alpha^2 k^2 \pm 2\sqrt{V_z^2\Delta^2 + \tilde{\epsilon}^2(V_z^2 + \alpha^2 k^2)}, \tag{50}$$

where $\tilde{\epsilon} = \eta k^2 - \mu$. Setting $k=0$, it can be seen that

$$E_0^2 = (V_Z \pm \sqrt{\Delta^2 + \mu^2})^2, \tag{51}$$

which vanishes as C_0 becomes zero, as expected. Recent work[61] has shown that the quantity C_0 is the Pfaffian of the BdG Hamiltonian at $k=0$, $\{C_0 = Pf[H_{\mathrm{BdG}}(k=0)\sigma_y\tau_y]\}$. The sign of C_0, which determines whether the phase of the superconductor is non-Abelian or not has been shown to be related[61] to the parity of the first Chern number topological invariant describing time-reversal broken topological superconductors.[62–65]

The phase diagram of the spin-orbit-coupled semiconductor system can be understood from Fig. 4, which gives the variation in the quasiparticle gap versus the Zeeman splitting. One knows from topological stability of the Majorana fermion mode that, due to its nondegeneracy, the Majorana state is protected as long as the bulk gap does not close as one moves through the parameter space. In Fig. 4, the gap closes (at the wave vector $k=0$) for the Zeeman splitting corresponding to $V_z^2 = V_{zc}^2 = \Delta^2 + \mu^2$. The phase with $V_z > V_{zc}$ supports the nondegenerate Majorana state while the phase with $V_z < V_{zc}$ does not. These two regions are separated by a gapless point in the parameter space, which signifies a topological quantum phase transition. The quantum phase transition is topological since the superconducting order on both sides is explicitly s wave and the two phases differ only by the topological properties such as Majorana modes in defects and boundaries. A similar phase transition involving Majorana fermions in an artificial laser generated (vortex) in the spin-orbit coupling with a critical Zeeman field satisfying a similar condition has previously been reported in the context of cold atoms.[51]

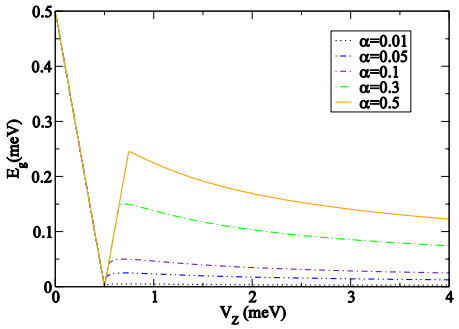

FIG. 4. (Color online) Quasiparticle gap versus Zeeman coupling for various values of spin-orbit interaction α. The strength of the spin-orbit coupling in the inset is such that $\alpha=0.3$ corresponds to 0.1 eV Å. The other parameters are taken to be $\Delta=0.5$ and $\mu=0.0$. The gap vanishes at the critical value $V_z = \sqrt{\Delta^2 + \mu^2}$. The spin-orbit coupling has negligible effect below this critical point and the superconducting gap is of a conventional s-wave type. Above the critical value and in the absence of spin-orbit coupling, the superconducting gap is destroyed by the Zeeman coupling. Spin-orbit coupling opens up a gap in this phase leading to re-entrant superconductivity which is topological.

VIII. COMPETITION BETWEEN SUPERCONDUCTIVITY AND ZEEMAN SPLITTING

The proposal to realize Majorana fermion modes in spin-orbit-coupled semiconductor system involves the introduction of a large Zeeman potential. In general, a Zeeman splitting is known to compete with and eventually destroy superconductivity. To understand better the competition between the Zeeman splitting and superconductivity in a spin-orbit-coupled semiconductor, we first consider the case without spin-orbit coupling. This case is described by the BdG Hamiltonian

$$H_{\mathrm{BdG}} = (\eta k^2 - \mu)\tau_z + V_z\sigma_z + \Delta\tau_x. \tag{52}$$

The dispersion relation of this Hamiltonian is $E_k = \pm V_z \pm \sqrt{\Delta^2 + \tilde{\epsilon}^2}$. In this case, with $V_z=0$, we obtain a conventional proximity-induced s-wave superconductor with no Majorana phase. As V_z increases above $\sqrt{\mu^2 + \Delta^2}$ the quasiparticle gap of the system closes and one obtains a metal with a Fermi momentum k_F given by $\eta k_F^2 = \mu \pm \sqrt{V_z^2 - \Delta^2}$. This is the well-known Chandrasekhar-Clogston limit[66,67] where strong Zeeman splitting suppresses the superconducting quasiparticle gap. This suppression is due to the fact that, in the spin-polarized regime ($|V_Z| > |\mu|$), a small pairing potential cannot open a s-wave superconducting gap since the latter couples opposite spins.

The BdG Hamiltonian at k_F is doubly degenerate and is given by

$$H_{\mathrm{BdG}} = \sqrt{V_z^2 - \Delta^2}\tau_z + V_z\sigma_z + \Delta\tau_x. \tag{53}$$

The degeneracy of the above Hamiltonian at the gapless point, which arises from the particle-hole symmetry, is lifted

by the Rashba spin-orbit coupling term $\alpha k_F \sigma_x \tau_z$ in the semiconductor to lowest order in perturbation theory. This yields a topological superconductor with a gap given by

$$E_g \approx 2\alpha k_F \frac{\Delta}{V_z} \tag{54}$$

for $\alpha k_F \ll V_Z$.

Considering the gap as a function of the Zeeman splitting (Fig. 4), it is clear that, for Zeeman splitting below the critical value $V_Z < \sqrt{\Delta^2+\mu^2}$, the superconductivity is nontopological in nature. The topological superconducting phase that supports Majorana fermions is created by the application of a Zeeman splitting to *suppress the conventional pairing potential*. In this regime, the spin-orbit coupling can open up a gap resulting in a re-entrant superconducting phase. However, as is evident from the previous discussions, the re-entrant superconductivity is unconventional (topological) in the sense that it supports Majorana fermions.

IX. TOPOLOGICALLY PROTECTED EDGE STATES AT INTERFACES

One of the signatures of a topological phase is the existence of gapless edge states which are inextricably linked to bulk topological properties such as Majorana modes in vortices.[4,68–71] The spin-orbit-coupled semiconductor structure introduced in Sec. II can be shown to have gapless edge states using methods similar to the ones described in the previous sections. Furthermore it turns out that this approach to analyze the existence of Majorana edge modes does not impose additional requirements such as rotational invariance that were critical for the demonstration of a Majorana solution in a vortex. Therefore, this method can be used to examine the question of the existence of Majorana edge modes even in the heterostructures with more general forms of spin-orbit coupling proposed by Alicea[56] where the Zeeman splitting can be introduced by an in-plane magnetic field.

A. BdG Hamiltonians for edges

Edges can be created in the semiconductor heterostructure by varying a parameter of the Hamiltonian such as μ, V_Z, or Δ perpendicular to the edge of a surface. Without loss of generality we can consider an edge that is perpendicular to the direction $\hat{y}$. Because of translational symmetry along the edge, the resulting edge BdG Hamiltonian has k_x as a parameter. The momentum parameter k_x transforms as $k_x \to -k_x$ under the particle-hole transformation. Therefore, a nondegenerate Majorana mode can only exist for $k_x=0$.

Fixing $k_x=0$ reduces the two-dimensional edge problem to a one-dimensional BdG Hamiltonian for a single-band semiconductor with spin-orbit coupling (assumed to be linear in the momentum k_y), which in general can be written as

$$H_{\mathrm{BdG}} = [-\eta\partial_y^2 - \mu(y)]\tau_z + V_z \boldsymbol{\sigma}\cdot\hat{\boldsymbol{B}} + \imath\alpha\partial_y \hat{\boldsymbol{\rho}}\cdot\boldsymbol{\sigma}\tau_z + \Delta(y)\cos\phi\tau_x + \Delta(y)\sin\phi\tau_y, \tag{55}$$

where the unit vector $\hat{\boldsymbol{B}}$ is the direction of the effective Zeeman field and the unit vector $\hat{\boldsymbol{\rho}}$ characterizes the spin-orbit coupling. Using the spin-rotation transformations on H_{BdG}, we can choose $\hat{\boldsymbol{\rho}}=\hat{\boldsymbol{y}}$ without loss of generality. This yields the Hamiltonian

$$H_{\mathrm{BdG}} = [-\eta\partial_y^2 - \mu(y)]\tau_z + V_z \boldsymbol{\sigma}\cdot\hat{\boldsymbol{B}} + \alpha(\imath\sigma_y)\tau_z\partial_y + \Delta(y)\cos\phi\tau_x + \Delta(y)\sin\phi\tau_y, \tag{56}$$

which is invariant under spin rotations about the y axis. Therefore without loss of generality we can reduce the above Hamiltonian to

$$H_{\mathrm{BdG}} = [-\eta\partial_y^2 - \mu(y)]\tau_z + V_Z(\cos\nu\sigma_z + \sin\nu\sigma_y) + \alpha(\imath\sigma_y)\tau_z\partial_y + \Delta(y)\cos\phi\tau_x + \Delta(y)\sin\phi\tau_y. \tag{57}$$

Nondegenerate Majorana spinor solutions are of the form $\Psi=(u,\imath\sigma_y u^*)$ and are completely determined by the two-spinor u. This fact was used to obtain the Majorana solutions for vortices to reduce the BdG equation from a 4×4 system of equations to a 2×2 system of equation. However, this reduction procedure required the BdG Hamiltonian to be real which is not the case for general forms of spin-orbit coupling and Zeeman splitting. The BdG equation for the zero-energy mode $H_{\mathrm{BdG}}\Psi=0$ may be reduced to an equation for u as

$$\{[-\partial_y^2 - \mu(y)] + V_Z(\cos\nu\sigma_z + \sin\nu\sigma_y) + \alpha(\imath\sigma_y)\partial_y\}u + \Delta(y)e^{\imath\phi}(\imath\sigma_y)u^* = 0. \tag{58}$$

This equation is not real but may be reduced to a system of real equations by writing $u=u_R+\imath u_I$ and taking the real and imaginary parts of the resulting equation giving a pair of equations of the form

$$\{[-\partial_y^2 - \mu(y)] + V_Z\cos\nu\sigma_z + \alpha(\imath\sigma_y)\partial_y + \Delta(y)\cos\phi(\imath\sigma_y)\}u_R - [\Delta(y)\sin\phi - V_Z\sin\nu](\imath\sigma_y)u_I = 0, \tag{59}$$

$$\{[-\partial_y^2 - \mu(y)] + V_Z\cos\nu\sigma_z + \alpha(\imath\sigma_y)\partial_y - \Delta(y)\cos\phi(\imath\sigma_y)\}u_I + [\Delta(y)\sin\phi - V_Z\sin\nu](\imath\sigma_y)u_R = 0. \tag{60}$$

The above pair of equations is similar to the pair of equations obtained for the two $\lambda=\pm1$ channels except that earlier the two channels were decoupled. For $\Delta(y)$ independent of y, the two channels can also be decoupled by choosing ϕ such that $\Delta(y)\sin\phi=V_Z\sin\nu$. In what follows, we will make this choice and also replace $V_Z\cos\nu\to V_Z$ and $\Delta\cos\phi\to\Delta$. This results in a reduced BdG equation for the $E=0$ reduced spinor $\Psi_0(y)$,

$$\begin{pmatrix} -\eta\partial_y^2 + V_z - \mu(y) & \lambda\Delta(y) + \alpha\partial_y \\ -\lambda\Delta(y) - \alpha\partial_y & -\eta\partial_y^2 - V_z - \mu(y) \end{pmatrix}\Psi_0(y) = 0, \tag{61}$$

where $\lambda=\pm1$.

An edge in a two-dimensional system of the type considered above is defined by requiring some parameter of the Hamiltonian to vary across the edge situated at $y=0$. We take this parameter to be constant for $y<0$ and $y>0$. In this case, our previous approach can be applied in a way even simpler than the application to the vortex problem, since the solutions on both sides of the interface at $y=0$ can be approximated as a sum $\Psi_0(y)=\Sigma_n a_n e^{-z_n y}u_n$ where, as in the interior

of the vortex (but far from the vortex core) [Eq. (24)],

$$\begin{pmatrix} -\eta z_n^2 + V_z - \mu & \lambda\Delta - z_n\alpha \\ -\lambda\Delta + z_n\alpha & -\eta z_n^2 - V_z - \mu \end{pmatrix} u_n = 0. \quad (62)$$

Similar to the vortex case, in the topological phase $C_0=(\Delta^2+\mu^2-V_Z^2)<0$, there are three values of z_n such that $\mathrm{Re}(z_n)<0$, while in the nontopological phase $C_0>0$, there are only two solutions in a given λ channel. The coefficients a_n in the solution are determined by matching the boundary conditions on $\Psi_0(y)$ at $y=0$. The coefficient C_0, written in terms of the original parameters of the wire, reduces to

$$C_0 = \Delta^2 \cos^2\phi + \mu^2 - V_Z^2 \cos^2\nu = \Delta^2 + \mu^2 - V_Z^2 \quad (63)$$

and is not affected by the ϕ and ν parameters that were introduced to make the BdG Hamiltonian real. The procedure of reducing the BdG Hamiltonian to a real Hamiltonian introduces an additional constraint in the form of a minimum value of Δ required to be in a gapped topological phase i.e., $|\Delta|>|V_Z \sin\nu|$.

B. Chiral edge states

Based on analogy with FQH state and chiral p-wave superconductors, one expects a chiral gapless state confined to the edge of the semiconductor heterostructure. An edge can be created in such structures by raising the chemical potential μ toward the edge such that electrons stay confined inside the system. Therefore, an edge of a system confined to $y>0$ is defined by $\mu(y)=\mu$ for $y>0$ and $\mu(y)=\infty>|V_z|$ for $y<0$. In these structures we assume that $\Delta(y)=\Delta$ is independent of y.

The BdG equation for $y>0$ and $k_x=0$ now reduces to a 2×2 system of equations,

$$[-\eta\partial_y^2 - \mu + V_z\sigma_z - \imath\alpha\sigma_y\partial_y + \imath\lambda\sigma_y\Delta]\psi(y) = 0, \quad (64)$$

where

$$\psi(y) = \begin{pmatrix} u_\uparrow(y) \\ u_\downarrow(y) \end{pmatrix}. \quad (65)$$

In order to solve a semi-infinite system we make a plane-wave trial solution ansatz,

$$\psi(y) = e^{-zy}\begin{pmatrix} u_\uparrow \\ u_\downarrow \end{pmatrix}, \quad (66)$$

where z must now satisfy

$$\begin{pmatrix} -\eta z^2 + V_z - \mu & \lambda\Delta - z\alpha \\ -\lambda\Delta + z\alpha & -\eta z^2 - V_z - \mu \end{pmatrix}\begin{pmatrix} u_\uparrow \\ u_\downarrow \end{pmatrix} = 0. \quad (67)$$

As in the case of the vortex [Eq. (25)], for $V_z^2>(\Delta^2+\mu^2)$ there are three solutions on the right half of the complex z plane and one solution on the left half for $\lambda=-1$. The situation is opposite for $\lambda=1$. Solutions with $\mathrm{Im}(z)>0$ are physical on the left edge of the system while $\mathrm{Im}(z)<0$ is physical on the right edge of the system. Thus for $\lambda=-1$ there are three physical solutions on the left edge of the system which is the exact number needed to make the two-component spinor vanish at the left edge. Consequently, there is a localized zero mode at the left edge of the system in the $\lambda=-1$ channel. Similarly there is a localized zero mode at the right edge of the system in the $\lambda=+1$ channel. Finally, for $V_z^2<(\Delta^2+\mu^2)$, there are no zero-energy solutions at either edge since there are only two physical solutions at each edge which is insufficient to match the boundary conditions. Since the wave function is confined to the edge, we expect the boundary conditions $\Psi_{0,\uparrow}(0)=\Psi_{0,\downarrow}(0)=0$, which together with normalization lead to three constraints. As mentioned before, in the topological phase we obtain three a_n coefficients corresponding to the three normalizable solutions in the interior. Therefore, there is a unique zero-energy state resulting from a matching of the boundary conditions. This state is a Majorana mode for the end point of the nanowire in the topological phase ($C_0<0$), which disappears when we tune the wire through a phase transition to $C_0>0$. The Majorana modes at the edges discussed above only occurred at $k_x=0$. The complete spectrum of the edge is obtained by considering the BdG Hamiltonian at small $k_x\neq 0$ using the $k\cdot p$ perturbation theory. To lowest order in k_x, the Nambu Spinor wave function can be approximated as $\Psi_{k_x}(x,y)\approx e^{ik_x x}\Psi_0(y)$ with an energy $E_{k_x}=vk_x$, where $v=\langle\Psi_0|\sigma_y\tau_z|\Psi_0\rangle$.

A similar chiral Majorana wire is obtained by considering an edge between the topological phase $C_0<0$ and $C_0>0$ where $\mu(y)$ is constant but $V_Z(y)=0$ for $y>0$. In that case there are five constraints to match as in the vortex case, and there are five coefficients, three arising from the topological phase at $y<0$ and two from the nontopological phase $y>0$.

C. Nonchiral Majorana edge states

Now we consider the junction of a pair of topological superconducting islands with phases ϕ and $\phi'=\pi-\phi$ which is a geometry that is of particular interest to TQC architechtures.[37,52] For such a choice of phases, the effective pairing potential in $\Delta\cos\phi(x)$ is a step function given by $\Delta(x)=\Delta\cos\phi$ for $x<0$ and $\Delta(x)=-\Delta\cos\phi$ for $x>0$. As before we then replace $\Delta\cos\phi\to\Delta$. Focusing on the $k_x=0$ particle-hole symmetric momentum for the edge, solutions for $x<0$ and $x>0$ can be expanded in terms of spinor functions given in Eq. (66) which is written in terms of eigenvalues z and eigenvectors satisfying Eq. (67). Normalizable solutions must now be composed of superpositions of exponentials with $\mathrm{Re}(z)<0$ for $y<0$ and $\mathrm{Re}(z)>0$ for $x>0$. We note at this point that the equations for $x>0$ and $x<0$ differ by a change in sign of $\Delta(x)$ across the interface which corresponds to a change in sign of z. Thus, as before for $\lambda=-1$, in the topological phase we have three values of z such that $\mathrm{Re}(z)>0$ for $x>0$ and three values such that $\mathrm{Re}(z)<0$ for $x<0$. Following the boundary condition matching argument of the last section, for the π junction there are six states at $x=0$ to compose wave functions at $x=0$ which need to satisfy five constraints. Therefore, generically there will be a pair of zero-energy modes satisfying these equations.

It might appear that, unlike the case for the chiral edge states, the pair of Majorana states cannot be topologically protected. In the case of the TI/SC interface,[37] the existence

of such a pair of nonchiral Majorana edge modes at a phase difference π was a consequence of time-reversal symmetry which is broken here. In our calculation we find that because of this time-reversal breaking, the pair of degenerate zero modes may occur at a phase difference of $\pi-2\phi$. In fact, by considering the evolution of the Andreev bound-state spectrum in the junction as a function of phase difference,[57] it is possible to show that even though the Majorana nature of the pair of nonchiral Majorana modes is not topologically protected, it is not possible to eliminate the zero modes all together. The zero crossing of the nonchiral Majorana modes may only be shifted to different values of phase by time-reversal breaking perturbations. This is a result of the fact that the two-particle-hole symmetry related branches of the Andreev bound-state spectrum differ by fermion parity. Therefore, even though an infinitesimal perturbation can lift the degeneracy of the two zero modes at some value of phase difference $\delta\phi$, it can only do so by shifting the crossing to a neighboring value of $\delta\phi$. Similar to the chiral edge modes one can use the $k\cdot p$ perturbation theory to construct a pair of linearly dispersing modes from the pair of zero-energy states at $k_y=0$.

X. MODEL CALCULATIONS OF PROXIMITY EFFECTS IN SUPERCONDUCTOR-SEMICONDUCTOR-MAGNETIC INSULATOR HETEROSTRUCTURES

In this section we study, starting from a microscopic tight-binding model, the excitation spectrum of a semiconductor thin film sandwiched between an s-wave SC and a ferromagnetic insulator (MI). We determine the dependence of the effective SC gap and Zeeman splitting induced by proximity effects on the parameters that characterize the heterostructure model. We also calculate the dynamical contributions to a low-energy effective theory of the proximity effect and identify parameter regimes suitable for the experimental implementation of the semiconductor-based proposal of a platform for topological quantum computation.

To study the proximity effect in the SC-semiconductor-MI heterostructure, we consider the minimal microscopic model defined by the Hamiltonian

$$H_{\rm tot}=H_0+H_{\rm SC}+H_{\rm MI}+H_{\tilde{t}_S}+H_{\tilde{t}_M}. \tag{68}$$

The H_0 term describes the semiconductor thin film,

$$H_0=\sum_{i,j,\sigma}t_{ij}c^\dagger_{i\sigma}c_{j\sigma}+\frac{\alpha}{2}\sum_{i,\sigma,\sigma'}[c^\dagger_{i+\delta_x\sigma}(i\hat{\tau}_y)_{\sigma,\sigma'}c_{i\sigma'} - c^\dagger_{i+\delta_y\sigma}(i\hat{\tau}_x)_{\sigma,\sigma'}c_{i\sigma'}+{\rm H.c.}]+\sum_{i,\sigma}V(z_i)c^\dagger_{i\sigma}c_{i\sigma}, \tag{69}$$

where the first contribution describes hopping on a cubic lattice while the second represents a lattice model of the Rashba spin-orbit interaction. The hopping matrix elements are nonvanishing for nearest neighbors, $t_{ij}=-t_0$, and next-nearest neighbors, $t_{ij}=-t_1$, and we also include an on-site contribution $t_{ii}=\epsilon_0$ that shifts the bottom of the semiconductor spectrum to zero energy. The parameter α represents the Rashba coupling constant and $\delta_{x(y)}$ are nearest-neighbor displacements in the xy plane of a cubic lattice with lattice parameter a. The system is assumed to be infinite in the x and y directions and contains N planes perpendicular to the z direction. The quantities $\hat{\tau}_{x(y)}$ are Pauli matrices and $c^\dagger_{i\sigma},c_{i\sigma}$ are electron creation and annihilation operators, respectively. The last term represents an external bias potential that modify the on-site energies along the z direction.

For the superconductor we use a simple mean-field model defined by the Hamiltonian

$$H_{\rm SC}=-t_s\sum_{\langle i,j\rangle,\sigma}b^\dagger_{i\sigma}b_{j\sigma}+\epsilon_s\sum_{i,\sigma}b^\dagger_{i\sigma}b_{i\sigma}+\sum_i(\Delta b^\dagger_{i\uparrow}b^\dagger_{i\downarrow}+{\rm H.c.}), \tag{70}$$

where t_s represents the nearest-neighbor hopping on a cubic lattice and Δ is the mean-field s-wave SC order parameter. The SC and the semiconductor thin film have a planar interface perpendicular to the z direction. For clarity, the electron creation and annihilation operators inside the SC were denoted $b^\dagger_{i\sigma}$ and $b_{i\sigma}$, respectively.

The third term in Eq. (68) represents the ferromagnetic insulator which, again, is modeled at the mean-field level by the Hamiltonian

$$H_{\rm MI}=-\sum_{\langle i,j\rangle,\sigma}t_{m\sigma}a^\dagger_{i\sigma}a_{j\sigma}+\sum_{i,\sigma}\left(\epsilon_{m\sigma}-\sigma\frac{\Gamma}{2}\right)a^\dagger_{i\sigma}a_{i\sigma}. \tag{71}$$

The nearest-neighbor hopping is spin dependent and we consider the case $t_{m\downarrow}=-t_{m\uparrow}>0$. The spin-dependent on-site energy was divided into a contribution $\epsilon_{m\sigma}=\epsilon_{m0}+6t_{m\sigma}$ that places the top of the valence band and the bottom of the conduction band at the same energy ϵ_{m0} and a term proportional to the insulating gap Γ. The last two terms in Eq. (68) describe the coupling at the two interfaces, semiconductor-SC and semiconductor-MI, respectively,

$$H_{\tilde{t}_S}=-\sum_{\langle i,j\rangle,\sigma}\tilde{t}_S(b^\dagger_{i\sigma}c_{j\sigma}+{\rm H.c.}), \tag{72}$$

$$H_{\tilde{t}_M}=-\sum_{\langle i,j\rangle,\sigma}\tilde{t}_M(a^\dagger_{i\sigma}c_{j\sigma}+{\rm H.c.}). \tag{73}$$

The parameters $\tilde{t}_S$ and $\tilde{t}_M$ characterize the transparencies of the two interfaces and provide the energy scales for the coupling between the semiconductor thin film and the SC and MI, respectively. These energy scales are crucial for determining the strength of the proximity effects.

We diagonalize Eq. (68) numerically for a system with periodic boundary conditions along the x and y directions and a finite size along the z direction. The semiconductor, SC and MI contain N, N_s, and N_m planes, respectively. For the semiconductor thin film we consider $5\leq N\leq 20$ while N_s and N_m are typically on the order of several hundreds. For large systems, the proximity effects are independent on N_s and N_m and we explicitly checked that the values used in the calculations are within that regime. The hopping matrix elements for the semiconductor are $t_0=1.57$ eV and $t_1=0.39$ eV, which, for a cubic lattice with $a=5.5$ Å generate in the low-wavelength limit a small effective mass $m^*=0.04m_e$ characteristic of semiconductors such as InAs. The value of the

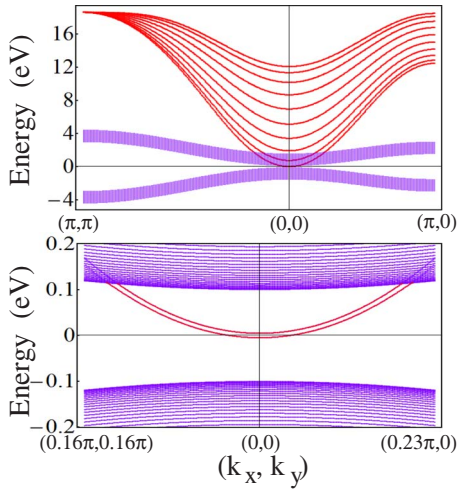

FIG. 5. (Color online) Band structure for a semiconductor-ferromagnetic insulator heterostructure described by Eqs. (68), (69), (71), and (73) with $N=10$ and $\tilde{t}_M=250$ meV. The red points (the wide bands in the upper panel) represent semiconductor states while the magenta bands (narrow bands in the upper panel) are ferromagnetic insulator states. The lower panel shows the low-energy behavior around $\mathbf{k}=0$. Notice the spitting of the semiconductor band at $\mathbf{k}=0$ due to the effective Zeeman term induced by ferromagnetic proximity effect.

Rashba coupling constant is $\alpha=18$ meV, corresponding to a strong spin-orbit coupling of the order 100 meV Å. For the SC, the hopping parameter is $t_s=0.35$ eV and $\Delta=1.5$ meV, while the magnetic insulator is described by $t_{m\downarrow}=-t_{m\uparrow}=0.36$ eV and a gap value $\Gamma=200$ meV. The coupling parameters $\tilde{t}_S$ and $\tilde{t}_M$ are varied and typically range within several hundreds millielectron volt.

A. Magnetic proximity effect

First, we turn on the coupling at the interface between the semiconductor and the MI. Figure 5 shows the spectrum of a slab containing a semiconductor thin film with $N=10$ atomic layers in contact with a MI. The coupling at the interface is $\tilde{t}_m=250$ meV. The semiconductor spectrum is characterized by ten strongly dispersive bands represented by red (dark gray) curves in the upper panel of Fig. 5. For an isolated semiconductor, these bands are weakly split by the spin-orbit interaction and are double degenerate at $\mathbf{k}=0$. However, as a result of the magnetic proximity effect, an effective Zeeman splitting removes this degeneracy. This is shown in the lower panel of Fig. 5 for the lowest energy mode that has the minimum inside the insulating gap. The induced Zeeman splitting is entirely a result of the exchange interaction between the MI and the SM layers and is not related to the magnetic field produced by the ferromagnetic MI. In fact, effective Zeeman splittings have been known to induced by antiferromagnetic insulators as well through a phenomenon commonly known as exchange bias.[72]

A natural question of practical importance concerns the dependence of the induced Zeeman splitting on the parameters of the model. To get a better intuition of the physics behind the proximity effect, we start with an analysis of the

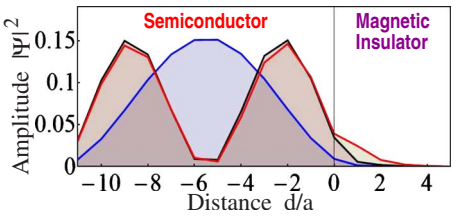

FIG. 6. (Color online) Dependence of the amplitude of low-energy states on the distance from the semiconductor-MI interface for three different sets of parameters. In order of increasing penetration depth into the MI: lowest semiconductor band ($n=1$) and $\tilde{t}_m=0.25$ eV (blue), second semiconductor band ($n=2$) and $\tilde{t}_m=0.25$ eV (black), and $n=2$, $\tilde{t}_m=0.5$ eV (red). For a given set of parameters, a certain fraction of each low-energy wave function penetrates the insulator leading to ferromagnetic correlations in the semiconductor thin film, i.e., to an effective Zeeman field induced by proximity effect.

structure of the wave functions of the relevant states. Consider a semiconductor state with an energy within the insulating gap Γ. When the semiconductor and the MI are coupled, the wave function describing this state will partly penetrate into the magnetic insulator, where it decays exponentially. These components of the wave functions inside the MI will acquire ferromagnetic correlations equivalent to an effective Zeeman field. Hence, the strength of the proximity effect is related to the fraction of the wave function that penetrates the MI. This qualitative picture of the proximity effect is illustrated in Fig. 6. In general, the fraction of the wave function that penetrates the insulator depends on three types of factors: (i) the properties of the quasi-two-dimensional parent system, in this case the semiconductor film, (ii) the properties of the insulating host system, and (iii) the coupling strength at the interface.

The first and last types of factors are qualitatively illustrated in Fig. 6. For example, by controlling the value of the on-site energy ϵ_0, i.e., chemical potential of the semiconductor, one can bring the minima of different semiconductor bands within the insulating gap. The profiles of the wave functions in the transverse direction (i.e., perpendicular to the film) depend on which band is inside the gap, as shown in Fig. 6 for the first two bands, $n=1$ and $n=2$. Furthermore, the fraction of the wave function that penetrates the insulator depends on its amplitude at the interface. This amplitude is significantly different for $n=1$ and $n=2$, hence one expects significantly different strengths of the proximity effect. Of course, the amplitude at the interface can be also modified by changing the size of the system (N) or by applying a bias potential $V(z)$ that can tilt the spectral weight toward or away from the interface. In addition to the amplitude at the interface, which is determined by the parameters of the semiconductor, the fraction of the wave function that penetrates the MI also depends on the slope at the interface. In essence, this slope is controlled by the coupling parameter $\tilde{t}_m$, as illustrated in Fig. 6. Finally, the parameters of the exponential decay inside the insulator, as well as the strength of the ferromagnetic correlations depend on the properties of the insulating host.

Next we proceed with a quantitative analysis of the induced Zeeman splitting and derive an effective low-energy

theory for the ferromagnetic proximity effect. We consider the situation when the states of the nth semiconductor band with wave vectors near $\mathbf{k}=0$ have energies inside the insulating gap. The states $\psi_{n\mathbf{k}\sigma}(\mathbf{r}_i)$ corresponding to vanishing spin-orbit coupling, $\alpha=0$, form a convenient basis for the low-energy Hilbert subspace of interest. Projecting the Hamiltonian H_0 onto this subspace we obtain

$$H_{0\text{eff}}(\mathbf{k}) = \begin{pmatrix} \dfrac{k^2}{2m^*} & \alpha(k_y - ik_x) \\ \alpha(k_y + ik_x) & \dfrac{k^2}{2m^*} \end{pmatrix}, \tag{74}$$

where m^* is an effective mass with a value slightly different from the effective mass corresponding to the 3D semiconductor model. The difference stems from the quasi-2D geometry of the system. The insulating degrees of freedom can be integrated out and replaced by an interface self-energy. When projected onto the low-energy subspace, this contribution becomes

$$\Sigma_{\sigma\sigma'}(\mathbf{k},\omega) = -\tilde{t}_m^2 |\psi_{n\mathbf{k}}(z_0)|^2 G^{(m)}_{\sigma\sigma'}(\mathbf{k},\omega;z_0+\delta_z), \tag{75}$$

where $G^{(m)}_{\sigma\sigma'}(\mathbf{k},\omega;z_0+\delta_z)$ is the Green's function of the magnetic insulator and $|\psi_{\mathbf{k}}(z_0)|^2$ the amplitude of the semiconductor wave function, both at the interface. From Eq. (75) one immediately notice that, neglecting dynamical effects, i.e., setting $\omega=0$, any induced Zeeman splitting has to be proportional with the amplitude of the wave function at the interface times the square of the interface transparency. For a vanishing bias potential, $V(z)=0$, the wave-function amplitude on the j atomic layer is proportional to $\sin^2[\pi nj/(N+1)]$ and the amplitude at the interface becomes

$$|\psi_{n\mathbf{k}}(z_0)|^2 = \frac{2\sin^2\left(\dfrac{n\pi}{N+1}\right)}{N+1}. \tag{76}$$

Note that, for clarity, we dropped the spin label, as the amplitude is spin independent. Also note that for large N the amplitude becomes $|\psi_{n\mathbf{k}}(z_0)|^2 \approx 2n^2\pi^2/(N+1)^3$. The dependence of the induced Zeeman splitting on the wave-function amplitude is shown in Fig. 7. As the film thickness $w=Na$ is increased, the value of the wave-function amplitude at the interface drops rapidly, as expected from Eq. (76). Due to the proximity effect, an effective Zeeman splitting creates a gap in the nth semiconductor band at $\mathbf{k}=0$,

$$\tilde{\Gamma} = E_{n2}(0) - E_{n2}(0), \tag{77}$$

where $E_{nj}(\mathbf{k})$ are the energies of the nth semiconductor band within the magnetic insulator gap (see lower panel of Fig. 5). The proportionality between the induced Zeeman gap $\tilde{\Gamma}$ (dots in Fig. 7) and the amplitude of the wave function (lines in Fig. 7) reveal the absence of significant dynamical effects, Eq. (75). This conclusion is further supported by the linear dependence $\tilde{\Gamma}$ on the square of the interface transparency, $\tilde{t}_m^2$, shown in Fig. 8. We emphasize that the effective coupling constant that determines the strength of the ferromagnetic proximity effect, $g_m = 2\tilde{t}_m^2 |\psi_n(z_0)|^2/\Lambda_m$, where Λ_m is a characteristic bandwidth for the magnetic insulator, can be tuned by: (a) modifying the semiconductor film thickness (see Fig. 7), (b) applying a bias voltage (see Figs. 7 and 8), and (c) changing the semiconductor-MI coupling (Fig. 8).

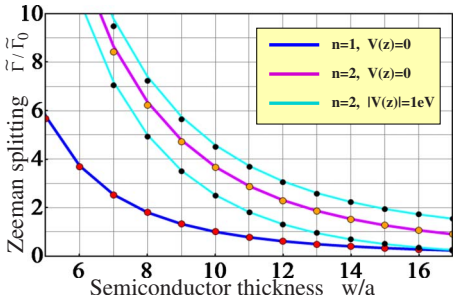

FIG. 7. (Color online) Dependence of the normalized effective Zeeman splitting on the semiconductor thickness for different sets of parameters (dots). The continuous lines represent the normalized wave-function amplitude at the interface (the Nth layer) $|\psi_n(N)|^2/|\psi_n(10)|^2$. The reference gap is $\tilde{\Gamma}_0=2.955$ meV. The wave-function amplitude in the absence of an applied bias, $V(z)=0$, is determined using Eq. (76) for $n=1$ (lower dark gray curve) and $n=2$ (upper dark gray curve), while for a linear bias $V(z)=V_0 z/w$ with $V_0=\pm 1$ eV the amplitude is determined numerically (light gray curves).

So far we have discussed the dependence of the proximity effect on the properties of the quasi-two-dimensional parent system and on the coupling strength at the interface. Next we briefly investigate the role of the insulating host system. We note that a full analysis would require a treatment of the magnetic insulator beyond the simple mean-field picture used here but this would not change the results obtained so far. Within our mean-field approximation, the MI Green's function from Eq. (75) can be easily evaluated,

$$G^{(m)}_{\sigma\sigma'}(\mathbf{k},\omega;z_0+\delta_z) = \delta_{\sigma\sigma'}\sum_{\nu}\frac{1}{\omega - E_{\nu\sigma}(\mathbf{k}) + i\eta}|\chi_{\nu\mathbf{k}\sigma}(z_0+\delta_z)|^2, \tag{78}$$

where $E_{\nu\sigma}(\mathbf{k})$ are the energies of the insulator bands and $\chi_{\nu\mathbf{k}\sigma}(z_0+\delta_z)$ the values of the corresponding eigenstates at

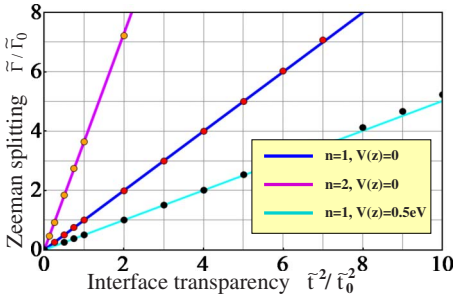

FIG. 8. (Color online) Dependence of the normalized Zeeman splitting on the interface transparency for a system with $N=12$ and different model parameters (dots). The straight lines are guide for the eyes. The reference interface coupling is $\tilde{t}_{m0}=250$ meV. The rather small deviations from a linear dependence indicate that dynamical effects are negligible, i.e., neglecting the frequency dependence in Eq. (75) is a good approximation.

the interface. It is convenient to express the Green's function in terms of the partial density of states $\rho_{\mathbf{k}\sigma}(\omega)=\Sigma_\nu \delta[\omega - E_{\nu\sigma}(\mathbf{k})]|\chi_{\nu\mathbf{k}\sigma}(z_0+\delta_z)|^2$. Within our model, this partial density of states becomes

$$\rho_{\mathbf{k}\sigma}(\omega)=\frac{2}{\pi\Lambda_\sigma}\sqrt{1-\left[\frac{\omega-\bar{E}_\sigma(\mathbf{k})}{\Lambda_\sigma}\right]^2} \tag{79}$$

with $\Lambda_\sigma=2|t_{m\sigma}|$ being half of the bandwidth in the insulating phase and $\bar{E}_\sigma(\mathbf{k})$ the energy values at the middle of the valence and conduction bands for a given wave vector parallel to the interface. At $\mathbf{k}=0$ we have $\bar{E}_\sigma(0)=-\mu-\sigma(\Gamma/2+\Lambda_\sigma)$. Note that $\rho_{\mathbf{k}\sigma}(\omega)$ vanishes for values of ω outside the bandwidth. Using Eq. (79), we obtain for the Green's function the expression

$$G^{(m)}_{\sigma\sigma}=\frac{2}{\Lambda_\sigma}\left[\frac{\omega-\bar{E}_\sigma}{\Lambda_\sigma}-\text{sign}(\omega-\bar{E}_\sigma)\sqrt{\left(\frac{\omega-\bar{E}_\sigma}{\Lambda_\sigma}\right)^2-1}\right]. \tag{80}$$

Note that the imaginary part of the Green's function vanishes for values of ω within the insulating gap. Also, because the energies of interest are much smaller than the insulator bandwidth, $\omega \ll \Lambda_\sigma$, we can neglect the frequency dependence in Eq. (80). Finally, within the static approximation, we obtain for the induced Zeeman splitting the expression

$$\tilde{\Gamma}=\Delta\tilde{\Gamma}_\downarrow-\Delta\tilde{\Gamma}_\uparrow,$$

$$\Delta\tilde{\Gamma}_\sigma=g_{m\sigma}\left\{\frac{-\mu-\sigma\left(\frac{\Gamma}{2}+\Lambda_\sigma\right)}{\Lambda_\sigma}+\sigma\sqrt{\left[\frac{-\mu-\sigma\left(\frac{\Gamma}{2}+\Lambda_\sigma\right)}{\Lambda_\sigma}\right]^2-1}\right\}, \tag{81}$$

where the effective coupling constant is $g_m=2\tilde{t}_m^2|\psi_n(z_0)|^2/\Lambda_\sigma$. To test the accuracy of this effective low-energy theory, we compare the values of the induced Zeeman splitting predicted by Eq. (81) with the numerical calculations. The results for various values of the insulating gap shown excellent agreement (see Fig. 9). Finally, we note that away from $\mathbf{k}=0$ the dispersion of the low-energy bands $E_{nj}(\mathbf{k})$ can be obtained by adding the self-energy contribution, Eq. (75), to the effective theory described by Eq. (74). Within the static approximation we have

$$H_{\text{eff}}(\mathbf{k})=\begin{pmatrix}\frac{k^2}{2m^*}-\frac{\tilde{\Gamma}}{2} & \alpha(k_y-ik_x)\\ \alpha(k_y+ik_x) & \frac{k^2}{2m^*}+\frac{\tilde{\Gamma}}{2}\end{pmatrix} \tag{82}$$

with $\tilde{\Gamma}$ given by Eq. (81). Explicit calculations for various sets of parameters show that this low-energy theory represents an excellent approximation for all $\mathbf{k}$ values of interest.

B. Superconducting proximity effect

Next, we turn our attention to the effects induced by the proximity of an *s*-wave superconductor on the semiconductor-MI heterostructure. The parameters of the semiconductor-MI interface are fixed with $\tilde{t}_m=250$ meV. We consider a semiconductor thin film with $N=10$ and create a new interface at the free surface of the semiconductor by coupling it to a SC with an *s*-wave gap Δ, i.e., we add the terms given by Eqs. (70) and (72) to the total Hamiltonian (68). The corresponding spectrum is shown in Fig. 10. The semiconductor band is split due to the ferromagnetic prox-

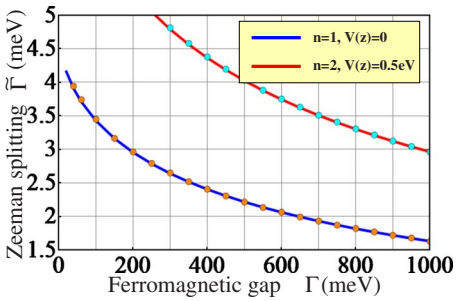

FIG. 9. (Color online) Dependence of the effective Zeeman splitting on the ferromagnetic insulator gap for the first ($n=1$, lower set of dots) and second ($n=2$, upper set of dots), semiconductor bands. For $n=2$ an additional linear bias is applied. The semiconductor has $N=10$ layers and the interface coupling with the ferromagnetic insulator is $\tilde{t}_m=250$ meV. The continuous lines are calculated using the effective low-energy theory described by Eq. (81). Notice the remarkable agreement between the low-energy theory and the exact results and the difference in energy scales between the insulating gap and the induced gap.

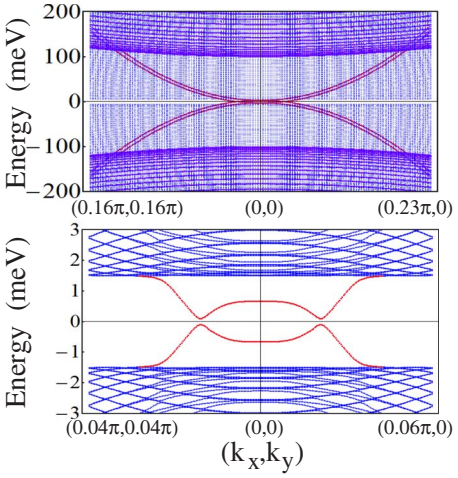

FIG. 10. (Color online) BdG spectrum of the full Hamiltonian (68) for a semiconductor thin film with $N=10$ sandwiched between a MI ($\Gamma=0.2$ eV, $\tilde{t}_m=250$ meV, and $\tilde{\Gamma}=2.95$ meV) and an *s*-wave SC ($\Delta=1.5$ meV and $\tilde{t}_s=130$ meV). The red points (highly dispersive bands inside the MI and SC gaps) represent states that reside (mostly) within the semiconductor, magenta designates the MI bands (upper panel, dark gray bands with a 0.2 eV gap), while the SC states are blue (upper and lower panels, bands with a 3meV gap), while SC states are blue (upper and lower panels, bands with a 3meV gap). Due to the effective Zeeman filed, the semiconductor bands are split and only one crosses the chemical potential (see upper panel). As a result of the superconductor proximity effect, a small gap opens at the crossing points (see lower panel).

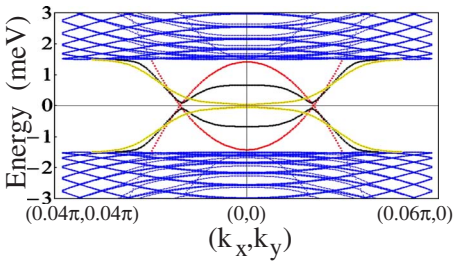

FIG. 11. (Color online) Dependence of the low-energy spectrum on the coupling between the semiconductor and the SC: $\tilde{t}_s=0$ (red, maximum gap at $\mathbf{k}=0$), $\tilde{t}_s=130$ meV (black, intermediate gap at $\mathbf{k}=0$), and $\tilde{t}_s=190$ meV (yellow, small gap at $\mathbf{k}=0$). The semiconductor film has $N=10$ layers and is also coupled (at the opposite surface) to a ferromagnetic insulator ($\tilde{t}_m=250$ meV). A proximity-effect-induced superconducting gap opens at finite k. As $\tilde{t}_s$ is increased, the minimal gap shifts to lower wave vectors and rest increases, then decreases and eventually vanishes at a critical coupling before opening again (see also Fig. 12).

imity effect and the chemical potential is tuned so that it crosses only the lower energy mode. When the coupling to the SC is turned on, a small gap opens at low energies due to the SC proximity effect (see Fig. 10 lower panel).

Before a quantitative analysis, let us illustrate qualitatively the behavior of the proximity-induced SC gap. Figure 11 shows the low-energy spectrum for three different values of the coupling constant $\tilde{t}_s$. For $\tilde{t}_s=0$ (red line, maximum gap at $\mathbf{k}=0$) the BdG spectrum is gapless. A nonvanishing interface coupling opens a small gap at the crossing points. The value of this finite wave-vector gap increases with $\tilde{t}_s$ but the gap at $\mathbf{k}=0$ decreases. (black line, intermediate gap at $\mathbf{k}=0$). Eventually, at a critical value $\tilde{t}_{\mathrm{SC}}$ the gap vanishes at $\mathbf{k}=0$, before opening again for larger couplings (yellow curve, small gap at $\mathbf{k}=0$). This closing of the induced gap signals the presence of a quantum phase transition.[52]

In order to understand this behavior, it is useful to develop an effective low-energy theory for the SC proximity effect. As shown previously,[42,43] dynamical corrections are crucial in capturing the low-energy physics in this case, in contrast to the ferromagnetic proximity effect. Using the results obtained in Refs. 42 and 43, the Green's function describing the low-energy physics of the heterostructure can be written as

$$-G^{-1}=(\xi_k+\lambda_k\sigma_+ +\lambda_k^*\sigma_-)\tau_z+\frac{\tilde{\Gamma}}{2}\sigma_z+\frac{g_s\Delta}{\sqrt{\Delta^2-\omega^2}}\tau_x - \omega\left(1+\frac{g_s}{\sqrt{\Delta^2-\omega^2}}\right), \tag{83}$$

where $\xi_k=k^2/2m^*-\mu$, $\tilde{\Gamma}$ is given by Eq. (81), $\lambda_k=\alpha(k_y-ikx)$, and the effective coupling is $g_s=2\tilde{t}_s^2|\psi(z_s)|^2/\Lambda_s$. The wave-function amplitude is evaluated at the semiconductor-SC interface and $\Lambda_s=2t_s$ is half of the SC bandwidth. The low-energy spectrum can be obtained by solving the corresponding BdG equation, $\mathrm{Det}(G^{-1})=0$. Explicitly, we have

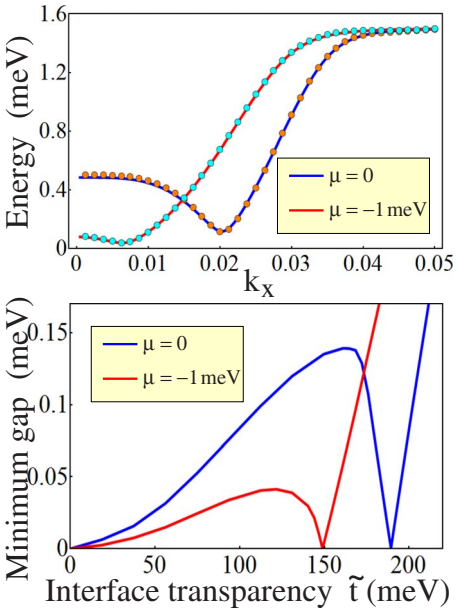

FIG. 12. (Color online) Upper panel: comparison between the solution of the effective low-energy theory given by Eq. (84) (lines) and the numerical solution of Hamiltonian (68) (dots) for two values of the chemical potential, $\mu=0$ (minimum gap at $k_x\approx 0.021/a$ and $\mu=-1$meV (minimum gap at $k_x\approx 0.007/a$. Only positive energies are shown. The semiconductor film ($N=10$) is coupled to both a ferromagnetic insulator ($\tilde{t}_m=250$ meV) and an s-wave SC ($\tilde{t}_s=200$ meV). Lower panel: dependence of the induced minimum gap on the SC interface transparency. The vanishing of the gap at a critical value $\tilde{t}_{\mathrm{SC}}(\mu)[\tilde{t}_{\mathrm{SC}}(0)\approx 188$ meV, $\tilde{t}_{\mathrm{SC}}(-1)\approx 148$ meV] reflects a quantum phase transition between a topologically nontrivial SC (at small values of $\tilde{t}_s$) and a trivial s-wave SC (at large couplings).

$$\omega^2\left(1+\frac{g_s}{\sqrt{\Delta^2-\omega^2}}\right)^2=\frac{\tilde{\Gamma}^2}{4}+\xi^2+|\lambda_k|^2+\frac{g_s^2\Delta^2}{\Delta^2-\omega^2} -2\sqrt{\xi_k^2\left(\frac{\tilde{\Gamma}^2}{4}+|\lambda_k|^2\right)+\frac{\tilde{\Gamma}^2}{4}\frac{g_s^2\Delta^2}{\Delta^2-\omega^2}}. \tag{84}$$

A comparison between the solution of Eq. (84) and the numerical calculations is shown in the upper panel of Fig. 12. The good agreement between the two calculations indicates that all the relevant ingredients have been incorporated into the effective low-energy theory. Note that the magnetic proximity-induced Zeeman splitting does not affect the proximity-induced superconducting pairing potential, unlike the case of nonproximity-induced superconductors. This is because the Zeeman potential is proximity induced and is proportional to the tunneling to the magnetic insulator, which vanishes at the superconductor since it is separated from the magnetic insulator by the semiconductor. This argument is further supported by the good agreement between the effective model and the numerical calculation. The dependence of the minimum gap on the interface coupling is shown in the lower panel of Fig. 12. Note that the critical value of $\tilde{t}_s$ at

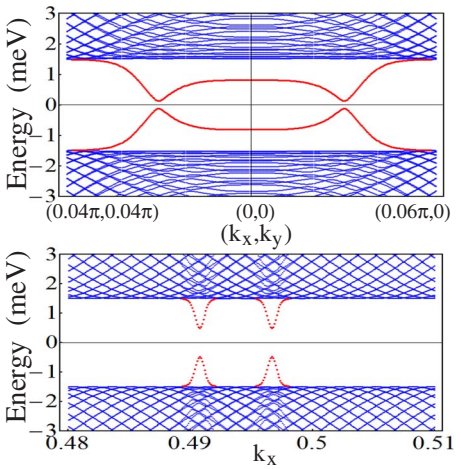

FIG. 13. (Color online) Details of the low-energy spectrum for the case when the $n=2$ semiconductor band has the minimum in the vicinity of the chemical potential. The semiconductor film has $N=10$ layers and the couplings at the interfaces with the ferromagnetic insulator and the SC are ($\tilde{t}_m=250$ meV) and ($\tilde{t}_s=200$ meV), respectively. The low-energy physics in the vicinity of $k=0$ (upper panel) is described by the effective theory given by Eq. (84) with a coupling constant g_s that includes the amplitude of the $n=2$ state at the interface. The $n=1$ semiconductor bands cross the chemical potential at larger values of k (lower panel) and are gaped due to SC proximity effect. Note that the gap at large wave vectors does not vanish at a critical coupling.

which the gap vanishes can be obtained from Eq. (84) by setting $\omega=0$. Explicitly we have

$$\tilde{t}_{\mathrm{SC}}(\mu)=\frac{\sqrt{t_s}}{|\psi(z_s)|}\left(\frac{\tilde{\Gamma}^2}{4}-\mu^2\right)^{1/4}. \tag{85}$$

The last question that we address in this section concerns the situation when a higher energy semiconductor band, $n>1$, has the minimum in the vicinity of the chemical potential. For concreteness, we consider the case $n=2$. The physics in the vicinity of $\mathbf{k}=0$ is similar with the case studied above. In addition, the $n=1$ bands cross the chemical potential at some large value of $\mathbf{k}$. Nonetheless, assuming that the partial density of states of the superconducting metal $\rho_{\mathbf{k}\sigma}(\omega)$ does not vary significantly with the wave vector, i.e., the effective mass of the metal is much greater than the effective mass of the semiconductor, the $n=1$ bands will be gapped and the induced gap is typically grater than the minimum gap near $\mathbf{k}=0$. Hence, the general conclusions of our analysis of the $n=1$ case hold for $n>1$. To illustrate this point, we show in Fig. 13 the relevant details of the low-energy spectrum for the case $n=2$.

XI. MAJORANA FERMION MODES IN ONE-DIMENSIONAL NANOWIRE

In the previous sections, we discussed how Majorana states may appear at vortices and edges of various two-dimensional spin-orbit-coupled semiconductor heterostructures. In this section, we show that Majorana fermions can also be realized in the much simpler one-dimensional nanowire set up (Fig. 14). In this setup we propose to study a semiconducting nanowire with a sizeable spin-orbit coupling (e.g., InAs) placed on an s-wave superconductor (e.g., Al). An in-plane magnetic field is used to create a Zeeman splitting in the nanowire,[57,73] which gives rise to the band structure shown in Fig. 14(b). The direction of the magnetic field (parallel or perpendicular to the length of the wire) that is required to open a gap in the nanowire depends on the exact direction of the spin-orbit coupling in the wire. For Rashba spin-orbit coupled wires, the direction of the spin-orbit coupling is perpendicular to the wire (which is the direction of the momentum). Therefore the in-plane magnetic field required to open a gap is parallel to the direction of the wire. As will become clear later, that if the magnetic field is not completely aligned with the direction of the wire, a topological superconductor exists only above a critical strength of the proximity effect $\Delta>|V_Z \sin \nu|$, where ν is the angle between the magnetic field and the direction of the wire. The chemical potential in the wire μ is assumed to be controlled by external gate voltages.

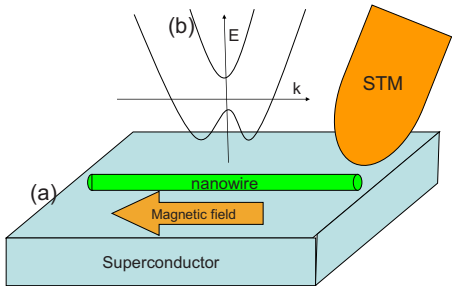

FIG. 14. (Color online) (a) Geometry to detect zero-energy Majorana fermions using STM spectroscopy on a semiconducting nanowire. The Zeeman splitting is induced by a parallel magnetic field while the chemical potential is controlled by an external gate (not shown). The Majorana fermion mode localized at the end of the nanowire gives rise to a zero-bias peak in the STM tunneling spectrum from the end. The tunneling spectrum from the bulk of the nanowire is gapped. (b) Band structure of the nanowire in the topological superconducting phase.

We argue below that, for the Zeeman splitting satisfying $V_Z>\sqrt{\mu^2+\Delta^2}$, a single nondegenerate zero-energy state exists at the end of the wire as the only low-energy bound state. The second quantized operator for this state is again a Majorana fermion operator. This mode can be detected as a zero-bias conductance peak in the scanning tunnel microscope (STM) tunneling spectrum. On reducing the Zeeman splitting so that $V_Z<\sqrt{\mu^2+\Delta^2}$, the Majorana mode, and hence the zero-bias conductance peak, should disappear from the tunneling spectrum.

The BdG Hamiltonian for a one-dimensional single-band semiconductor with spin-orbit coupling (which is linear in the momentum) in proximity to an s-wave superconductor (Fig. 14), can be written as

$$H_{\mathrm{BdG}}=[-\eta\partial_y^2-\mu(y)]\tau_z+V_z\boldsymbol{\sigma}\cdot\hat{\boldsymbol{B}}+\imath\alpha\partial_y\hat{\boldsymbol{\rho}}\cdot\boldsymbol{\sigma}\tau_z+\Delta\cos\phi\tau_x+\Delta\sin\phi\tau_y. \tag{86}$$

Here the unit vector $\hat{\boldsymbol{B}}$ gives the direction of the effective

Zeeman field and the unit vector $\hat{\boldsymbol{\rho}}$ characterizes the spin-orbit coupling. From inspection it is now clear that this Hamiltonian is formally identical to the Hamiltonian for the edge states, Eq. (56), at $k_x=0$. Therefore, from the solution of the chiral edge state at $k_x=0$ for the semiconductor thin film (Sec. IX B), we conclude that in the topological phase of the wire ($C_0<0$), the ends of the nanowire support localized zero-energy Majorana states. For magnetic fields $\hat{\boldsymbol{B}}$ that are not orthogonal to the direction of the spin-orbit coupling $\hat{\boldsymbol{\rho}}$, the proximity-effect-induced pairing potential Δ must exceed $\Delta > |V_Z \sin \nu|$, where $\sin \nu = \hat{B}\cdot\hat{\boldsymbol{\rho}}$ as discussed in Sec. IX.

STM detection of Majorana end modes in the nanowire

In the previous section, we showed that the end of a nanowire in the topological phase is characterized by a Majorana mode. The Majorana modes at the ends of a one-dimensional p-wave superconductor have been shown to lead to distinct signatures in the STM tunneling spectrum.[74,75] In what follows, we analytically and numerically calculate the STM conductance spectrum from one end of our semiconducting nanowire. We find that, for the Zeeman coupling satisfying ($V_Z > \sqrt{\Delta^2+\mu^2}$), this spectrum has a zero-bias conductance peak. The zero-bias peak disappears as the Zeeman splitting is reduced to satisfy ($V_Z < \sqrt{\Delta^2+\mu^2}$).

The tunneling spectrum of a superconducting system, similar to the tunneling conductance of normal systems, can be calculated using the Keldysh formalism of nonequilibrium Green's function[75] where the superconducting system is coupled to a tip which is initially in thermal equilibrium at a chemical potential μ_t, by an adiabatically increasing tunneling amplitude perturbation V. To calculate the current, we consider an STM tip state $\psi_\sigma^\dagger(x')$, where x' is restricted to the tip. The tunneling Hamiltonian between the STM tip and the superconducting wire can be written as

$$H_{tunnel} = \int dx dx' \sum_\sigma [V(xx')\psi_\sigma^\dagger(x')\psi_\sigma(x) + V^*(xx')\psi_\sigma^\dagger(x)\psi_\sigma(x')]. \tag{87}$$

The tunneling current can be related to the Keldysh Green's function of the combined system as[75]

$$I = \int dx dx' \sum_\sigma [V^*(xx')G_{\sigma\sigma}^{(K)}(xx') - V(xx')G_{\sigma\sigma}^{(K)}(x'x)]. \tag{88}$$

The Keldysh Green's function $G^{(K)}$ can be evaluated using the Dyson equation

$$G_{\sigma\sigma}^{(K)}(xx') = -G_{\sigma\sigma}^{(R)}(xx_1)V(x_1x_1')g_{\sigma\sigma}^{(K)}(x_1',x') - G_{\sigma\sigma}^{(K)} \times (xx_1)V(x_1x_1')g_{\sigma\sigma}^{(A)}(x_1',x'), \tag{89}$$

$$G_{\sigma\sigma}^{(K)}(x'x) = -g_{\sigma\sigma}^{(R)}(x'x_1')V^*(x_1x_1')G_{\sigma\sigma}^{(K)}(x_1,x) - g_{\sigma\sigma}^{(K)} \times (x'x_1')V^*(x_1x_1')G_{\sigma\sigma}^{(A)}(x_1,x), \tag{90}$$

where $g=(H_0-\omega)$ are the unperturbed Green's function and H_0 is the unperturbed Hamiltonian. Since the initial systems are in equilibrium, $g^{(K)}=(g^{(R)}-g^{(A)})\tanh\frac{\epsilon-\mu}{2T}$. Substituting these into Eq. (88), we get

$$I = \imath \int dx dx_1 d\omega \sum_\sigma \Gamma_\sigma(xx_1;\omega)\left[\tanh\frac{\omega-\mu_t}{2T}\{G_{\sigma\sigma}^{(R)}(xx_1;\omega) - G_{\sigma\sigma}^{(A)}(x,x_1;\omega)\} + G_{\sigma\sigma}^{(K)}(xx_1;\omega)\right], \tag{91}$$

where

$$\Gamma_\sigma(xx_1;\omega) = \int dx' dx_1' V^*(xx')V(x_1x_1')\rho_\sigma(xx_1;\omega) \tag{92}$$

and the tip spectral function at energy ω is given

$$\rho_\sigma(xx_1;\omega) = \imath[g_{\sigma\sigma}^{(A)}(x_1',x') - g_{\sigma\sigma}^{(R)}(x_1'x')]. \tag{93}$$

The exact Green's function in the superconductor can be calculated by integrating out the tip using Dyson's equation through the relation

$$G(xx_1;\omega) = g(xx_1;\omega) + g(xx_2;\omega)\Sigma(x_2x_3;\omega)G(x_3x_1;\omega), \tag{94}$$

where the tip induced self-energy is given by

$$\Sigma(xx_1;\omega) = \int_{-\infty}^{\infty} d\omega' \frac{\Gamma(xx_1;\omega')}{\omega-\omega'}, \tag{95}$$

$$\Sigma^K(xx_1;\omega) = \tanh\frac{\epsilon-\mu}{2T}\Gamma(xx_1;\omega). \tag{96}$$

The self-energy discussed above is for the normal Green's function, which is relevant for the tip. However to describe the superconductor, we need to consider the Nambu spinor Green's function at complex frequency ω. To be consistent with particle-hole symmetry, the self-energy in Nambu spinor notation is given by

$$\Sigma_{Nambu}(\omega) = \begin{pmatrix} \Sigma(\omega) & 0 \\ 0 & -\Sigma^*(-\omega^*) \end{pmatrix}. \tag{97}$$

The retarded and advanced self-energy are given at frequencies $\omega \pm \imath\delta$, respectively. The Dyson equations for the full Green's function $G=(H_{\mathrm{BdG}}-\omega)^{-1}$ in terms of the self-energy can be decomposed componentwise[76] as

$$G(\omega) = [1 - g(\omega)\Sigma(\omega)]^{-1}g(\omega), \tag{98}$$

$$G^{(K)} = (1 + G^{(R)}\Sigma^{(R)})g^{(K)}(1 + \Sigma^{(A)}G^{(A)}) + G^{(R)}\Sigma^{(K)}G^{(A)}. \tag{99}$$

Since the starting system is in equilibrium, $g^{(K)} = \tanh\frac{\epsilon-\mu}{2T}[g^{(R)}-g^{(A)}]$ and writing $(1+\Sigma G)=GH_0$, where H_0 is the unperturbed Hamiltonian, the latter equation can be reduced to

$$G^{(K)} = G^{(R)}\Sigma^{(K)}G^{(A)}. \tag{100}$$

Finally using the equilibrium constraint on the tip, one obtains the expression for the current[75]

$$I = \imath \int dx dx_1 d\omega \sum_\sigma \Gamma_\sigma(xx_1;\omega)\tanh\frac{\omega-\mu_t}{2T}\{G^{(R)}_{\sigma\sigma}(xx_1;\omega) - G^{(A)}_{\sigma\sigma} \times(x,x_1;\omega)\}. \quad (101)$$

To proceed further we must make assumptions about the Green's function for the STM tip. For a simple STM tip tunneling to the end of the nanowire, the tunneling can be assumed to occur between one point on the tip and the end of the wire. Furthermore, we can assume that the local density of states of the tip is a Lorentzian function $[(\omega-\mu_t)^2/W^2+1]^{-1}$, where W is the bandwidth about the tip. With these assumptions Γ is given by

$$\Gamma_\sigma(xx_1;\omega) = \frac{\Gamma}{(\omega-\mu_t)^2/W^2+1}\delta(x)\delta(x_1), \quad (102)$$

where μ_t is the chemical potential of the tip. The corresponding self-energy is given by

$$\Sigma(xx_1;\omega) = \frac{\Gamma W}{\omega - \imath\ \mathrm{sgn}\ \mathrm{Im}(\omega)W}, \quad (103)$$

where sgn $\mathrm{Im}(\omega)$ is the sign of the imaginary part of ω. The expression for the current with the above spectral density is given by

$$I = \imath\Gamma \int d\omega \sum_\sigma \tanh\frac{\omega-\mu_t}{2T}\frac{1}{\omega^2/W^2+1}\{G^{(R)}_{\sigma\sigma}(00;\omega) - G^{(A)}_{\sigma\sigma} \times(00;\omega)\}. \quad (104)$$

Using the identity $\tanh(\frac{\omega}{2T}) = 4\omega T\Sigma_{n\geq 0}\frac{1}{\omega^2+(2n+1)^2\pi^2T^2}$ and the fact $G^{(R)}$ and $G^{(A)}$ are analytic in the upper and lower half complex frequency planes, respectively, the ω integral can be replaced by a discrete sum over imaginary Matsubara frequencies as

$$I = T\Gamma \sum_{\sigma,n\geq 0}\frac{W^2}{W^2-(2n+1)^2\pi^2T^2}\mathrm{Re}\{G_{\sigma\sigma}[00;\mu_t+\imath(2n+1)\pi T]\} - T\Gamma W\sum_\sigma \tan\frac{W}{2T}\mathrm{Re}[G_{\sigma\sigma}(00;\mu_t+\imath W)]. \quad (105)$$

The second term in the expression for I regulates the singularity in the first term for $W\sim(2n+1)\pi T$. Using the Dyson equations [Eq. (98)], the expression for the Green's function G can be written in terms of the unperturbed nanowire Green's function $g(00;\omega)$ at complex frequency ω as

$$G_{\sigma\sigma}(00;\omega) = g[00;\mu_t+\imath(2n+1)\pi T][1-\Sigma[00;\mu_t+\imath(2n+1)\pi T])g[00;\mu_t+\imath(2n+1)\pi T]^{-1}|_{\sigma\sigma}. \quad (106)$$

The unperturbed nanowire Green $g(x,x'=0;\omega)$ at $x'=0$ satisfies the BdG equation

$$[\{-\eta\partial_x^2-\mu-V_g(x)-\imath\xi\sigma_y\partial_x-\}\tau_z+V_z\sigma_z+\Delta\tau_x-\omega] \times g(x,x'=a;\omega) = \delta(x-a) \quad (107)$$

for $x>-a$ with the boundary condition $g(x=-a,x'=0;\omega)=0$. Here the end of the wire has been taken to be at $x=-a$. Away from the boundary $x=-a$ and the contact point of the tip, $x=x'=0$, the Green's function can be expanded

$$g(xx'=0;\omega) = \sum_n \Psi_n C^\dagger_{n,-}e^{z_n x} \quad \text{for } x<0, \quad (108)$$

$$g(xx'=0;\omega) = \sum_{\mathrm{Re}(z_n)<0} \Psi_n C^\dagger_{n,+}e^{z_n x} \quad \text{for } x>0, \quad (109)$$

where

$$[\{-\eta z_n^2-\mu+\imath\xi\sigma_y z_n\}\tau_z+V_z\sigma_z+\Delta\tau_x-\omega]\Psi_n = 0 \quad (110)$$

and C are a set of vectors that are determined from boundary conditions. The quadratic eigenvalue problem in Eq. (110) can be reduced to a linear generalized eigenvalue problem by defining $\Phi=z\Psi$ as

$$z\Phi = -\frac{\xi}{\alpha}\sigma_y\Phi - \frac{1}{\alpha}[\{-\mu+V_z\sigma_z\tau_z\}+\imath\Delta\tau_y-E\tau_z]\Psi. \quad (111)$$

The coefficient vectors C are determined numerically by solving the boundary conditions

$$g(x=-a,x'=0;\omega) = 0, \quad (112)$$

$$-\tau_z[\partial_x g(x,x'=0;\omega)|_{x=0_+} - \partial_x g(x,x'=0;\omega)|_{x=0_-}] = \mathbf{1}, \quad (113)$$

$$g(x=0_-,x'=0;\omega) = g(x=0_+,x'=0;\omega). \quad (114)$$

The current $I(\mu_t=V)$ is calculated by using the Green's function $g(x=0,x'=0;\omega)$ in Eqs. (105) and (106). The conductance $\frac{dI}{dV}$ obtained by numerical differentiation of the current is shown in Fig. 15. In the units of the calculation, we have taken, $\eta=1$, $\Delta=0.5$, $\alpha=0.3$, $T=0.01$, $\Gamma=0.001$, and $W=5.0$. The Matsubara sum in Eq. (105) was taken to be $n_{\max}=500$ corresponding to $2\pi nT\sim 30$. As can be seen from panel (a) of the figure, the Majorana fermion mode at the end of the wire [in the non-Abelian phase, i.e., $V_Z>\sqrt{\Delta^2+\mu^2}=0.5$ meV] gives rise to a peak in the conductance at zero bias ($V=0$). The zero-bias peak decreases in strength for Zeeman much beyond the transition ($V_Z\gtrsim 0.75$) meV since the excitation gap starts to reduce in the topological phase at large Zeeman couplings [see Eq. (54)]. This weakens the tunneling of the Majorana to the tip since the Majorana state becomes more delocalized. Apart from the zero-bias peak, the bulk states in the nanowire also contribute to the STM conductance at bias voltages above the bulk energy gap. It is important to emphasize that, unlike p-wave superconducting nanowires, the tunneling spectrum of the present system (Fig. 15) has no state (other than the zero-energy Majorana state at the end) below the bulk energy gap Δ. Therefore the effective minigap at the ends is order the bulk energy gap (Δ). As the Zeeman splitting is lowered toward the critical value $V_{Z,c}=\sqrt{\Delta^2+\mu^2}=0.5$ meV, the bulk energy gap closes before reopening for $V_Z<\sqrt{\Delta^2+\mu^2}=0.5$ meV. For V_Z in this regime, the semiconductor is in a regular s-wave superconducting phase and there is no peak at zero bias. Instead there

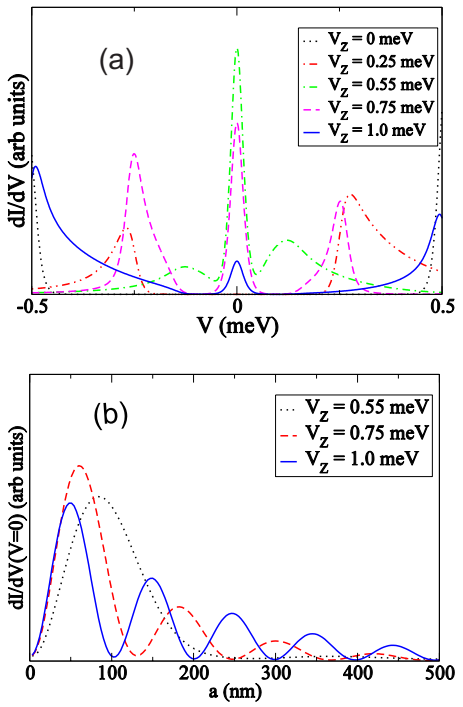

FIG. 15. (Color online) (a) Conductance dI/dV as a function of voltage $\mu_t = V$. For the plot we have taken $\eta = \hbar^2/2m^*$, where $m^* = 0.04m_e$ for InAs, $\Delta = 0.5$ meV for Nb, $\mu = 0$, $\alpha = 0.1$ eV Å, and $T = 100$ mK. The different values of V_Z in millielectron volt are given in the inset. The distance of the STM tip from the end of the nanowire has been taken as $a = 100$ nm. The plots for $V_Z > 0.5$ meV (corresponding to $B_x \sim 0.5$ T for InAs with $g_{\text{InAs}} \sim 35$) are in the topological phase and show a zero-bias peak while the plots for $V_Z < 0.5$ meV do not. (b) Position dependence of the zero-bias conductance in the topological phase. The amplitude of the zero-bias conductance is seen to be localized near the end of the wire and corresponds to the localized wave function of the Majorana mode at the end of the wire.

are two peaks which are associated with Van Hove singularities of the bulk quasiparticle spectrum. These peaks become sharper as the Zeeman potential is gradually lowered to zero.

STM spectroscopy can be used to not only verify the existence of the zero-energy Majorana states localized around the ends but also to study the spatial structure of the zero-energy wave functions. Panel (b) of Fig. 15 shows the zero-bias tunneling conductance as a function of distance a from one end of the wire. The calculation shows that the conductance vanishes at the end of the wire (the Majorana wave function must vanish at the end of the wire to satisfy the physical boundary condition). The zero-bias conductance then rises to a peak and oscillates with an envelope that decays away from the end of the wire. The decay length becomes longer as the in-plane magnetic field is tuned toward the critical value $V_{Z,c} = 0.5$ meV. No such zero-bias conductance should be observable for $V_Z < V_{Z,c}$. Thus, the STM experiment from the semiconducting nanowire provides one of the most experimentally feasible probes of Majorana fermions in condensed-matter systems.

The numerical results discussed in the previous paragraphs, Fig. 15, can be understood analytically in the limit that the STM tunneling strength is smaller than the thermal broadening ($\Gamma \ll T$). In this limit the current can be approximated as

$$I(\mu_t) \approx T\Gamma \sum_{\sigma} \sum_{n \geq 0} \text{Re}[g(00; \mu_t + \imath(2n+1)\pi T)_{\sigma\sigma}], \tag{115}$$

which can be cast into the more familiar expression for STM current

$$I(\mu_t) \approx \Gamma \sum_{\sigma} \int d\omega' A_{\sigma\sigma}(\omega') \tanh\left(\frac{(\omega' - \mu_t)}{2T}\right), \tag{116}$$

where the STM spectral function is given by $A_{\sigma\sigma'}(\omega) = \text{Im}[g_{\sigma\sigma'}(00;\omega)]$.[24] The corresponding conductivity

$$G(\mu_t) = \frac{dI(\mu_t)}{d\mu_t} = \Gamma \sum_{\sigma} \int d\omega' A_{\sigma\sigma}(\omega') \text{sech}^2\left(\frac{\mu_t - \omega'}{T}\right). \tag{117}$$

From the previous section, it is clear that the topological phase is characterized by a single Majorana state localized at the end. This zero-energy Majorana mode is expected to lead to a zero-bias peak in the tunneling spectrum. To see this we consider the 4×4 Nambu Green's function near $\omega = 0$ where it is dominated by the zero-energy pole as

$$g(00;\omega) \approx \frac{\Psi\Psi^\dagger}{\omega}, \tag{118}$$

where $\Psi^T = (u_\uparrow, u_\downarrow, u_\uparrow^*, u_\downarrow^*)$. The corresponding spectral function is

$$A_\sigma(\omega) \approx u_\sigma u_{\sigma'}^* \delta(\omega). \tag{119}$$

Using this in Eq. (117), the contribution of the zero-energy state to the conductance becomes

$$G(\mu_t) = \frac{dI(\mu_t)}{d\mu_t} = \tilde{\Gamma}\ \text{sech}^2\left(\frac{\mu_t}{T}\right), \tag{120}$$

where $\tilde{\Gamma} = \Gamma \Sigma_\sigma |u_\sigma|^2$.

Therefore STM spectroscopy provides a multifacted tool to study the properties of the topological quantum phase transition in the wire as the magnetic field is tuned from $B_x \sim 0$ to $B_x \sim 0.5$ T [which is significantly below the parallel critical field of thin-film Nb (Ref. 77)]. First the STM spectra away from the ends provides information about the induced superconducting gap in the wire, which diminishes as a function of applied magnetic field, goes to zero at the transition and then increases. For magnetic fields above the critical value, a zero-bias peak appears in the STM spectrum near the ends of the wire. Finally, STM can also be used to probe the spatial structure of the wave function of this Majorana mode. Thus, the STM experiment from the semiconducting nanowire provides one of the most experimentally feasible probes of Majorana fermions in condensed-matter systems.

XII. SUMMARY AND CONCLUSION

Let us first recapitulate the most important results contained in each section in this paper. In Secs. II and III we

analyze in detail the Hamiltonian and the BdG equations for a spin-orbit-coupled semiconductor in the proposed heterostructure geometry in the presence of a vortex. Here we provide all the mathematical details, left out in Ref. 52, which are necessary to conclusively establish the presence of a nondegenerate Majorana mode at the vortex core. In Sec. IV, we use the same formalism to establish the existence of a Majorana mode localized in a "vortexlike" defect in the spin-orbit coupling that can be artificially created in a spin-orbit-coupled atomic system potentially realizable in an optical lattice. Here we find that, contrary to a previous treatment of the same problem,[51] the decay length of the zero-energy Majorana mode localized in the spin-orbit vortex is inversely proportional to the superconducting gap. Therefore, in the limit of vanishing superconducting gap, the Majorana mode will delocalize over the entire system. We then show in Sec. V how the same formalism can be used to demonstrate the existence of a Majorana fermion mode in a vortex on the surface of a 3D topological insulator, even though in this simpler case an exact solution of the BdG equations is already available.[37]

In Sec. VI, we confirm our approximate analytical calculations, which are indicative of the existence of the zero-energy modes in the vortices in the spin-orbit-coupled semiconductor, by a full numerical solution of the BdG equations setup on a sphere.[58] Here we obtain the full bound-state excitation spectrum for the BdG Hamiltonian relevant for a vortex-antivortex pair placed at the poles of a sphere.[58] In the non-Abelian phase of the semiconductor film, this calculation produces a pair of lowest energy states whose energy eigenvalues approach zero exponentially with the radius of the sphere. This indicates the presence of one exact zero-energy state on each vortex in the limit of infinite intervortex separation. The numerical calculations also show that the excitation gap above the zero-energy state, the minigap, can be made comparable to the induced s-wave gap Δ in the semiconductor film. This surprising result, which was obtained previously for the proximity-induced superconducting state on the surface of a TI,[42] is now extended to the spin-orbit-coupled semiconductor in this paper. The enhancement of the minigap increases the regime of temperature in which any non-Abelian quasiparticle is accessible in experiments by many folds (from $T \sim \frac{\Delta^2}{E_F}$ to $T \sim \Delta$). In Sec. VII we briefly discuss the parameter regime in which the non-Abelian topological state is the ground state in the semiconductor film. The associated topological quantum phase transition (TQPT), which can be accessed by varying any one of the three parameters—Zeeman coupling (V_z), chemical potential (μ), and the proximity-induced s-wave gap (Δ)—is a transition at which the excitation gap vanishes at wave vector $k=0$. In Sec. VIII, we analyze the interplay of the Zeeman coupling and the proximity-induced s-wave superconductivity in the presence of spin-orbit coupling. We show that, even though the Zeeman coupling can eliminate s-wave superconductivity in the absence of spin-orbit coupling, the latter can give rise to a *re-entrant* non-Abelian superconducting state despite the fact that $|V_z| > |\Delta|$. Apart from the zero-energy Majorana states in order parameter defects such as vortices, the non-Abelian topological state in the semiconductor film is also characterized by gapless Majorana modes at the sample edges. In Sec. IX, we use the same techniques employed in the earlier sections to demonstrate the existence of these edge modes, which turn out to be *chiral* Majorana modes because of the explicit breakdown of the time-reversal symmetry.

In Sec. X we study the proximity effects in superconductor-semiconductor-magnetic insulator heterostructures starting from a microscopic tight-binding model. The superconductor and the magnetic insulator are described at the mean-field level. We determine the excitation spectrum of a slab containing a semiconductor thin film sandwiched between an s-wave superconductor and a ferromagnetic insulator and identify the dependence of the induced gaps on the parameters of the model. In particular, we study the dependence of the effective Zeeman splitting and induced superconducting gap on the thickness of the semiconductor film, the applied bias potential and the strength of the coupling at the interfaces.

Finally, in Sec. XI we demonstrate the existence of zero-energy Majorana modes at the ends of a one-dimensional version of the spin-orbit-coupled semiconductor system—a semiconducting nanowire. It has been shown that it may be far simpler to experimentally realize Majorana fermions in the one-dimensional nanowire system because the Zeeman splitting can be induced by a modest in-plane magnetic field, obviating the need for a proximate magnetic insulator.[57,73] We find that the Majorana modes at the two ends of the nanowire can be probed by scanning tunneling microscope experiments. We show by explicit calculations that the Majorana modes at the ends of the nanowire give rise to zero-bias conductance peaks in the tunneling spectrum at the ends. These peaks disappear on lowering the Zeeman coupling so that the system settles into the nontopological superconducting state. Furthermore these zero-bias conductance peaks are found to be the only features at bias voltages below the induced superconducting gap in the nanowire. We believe that the observation of this zero-bias tunneling peak in the semiconductor nanowire is the simplest experiment proposed so far to unambiguously detect a Majorana fermion state in a condensed-matter system.

We note here that the Majorana fermions, being non-Abelian particles belonging to the $(SU_2)_2$ conformal field theory (i.e., the so-called "Ising anyon" universality class), cannot directly be used for universal fault-tolerant topological quantum computation (TQC).[4] They can serve as topologically protected quantum memory or can be used in quantum computation along with supplementary unprotected quantum gates requiring only small amounts of error corrections.[78] Since the topological protection for the semiconductor heterostructures in our work is very robust, with the energy gap providing the protection being on the order of the superconducting gap (1–10 K) itself, our proposed system could serve as an excellent quantum memory in TQC applications. In a recent development, Bonderson *et al.*[79] have shown that certain dynamic-topology-changing operations, which are feasible in our proposed semiconductor heterostructures, dubbed Ising sandwich heterostructures in Ref. 79, could allow fully fault-tolerant TQC to be carried out using our proposed systems. Thus, in addition to the funda-

mental significance of the possible non-Abelian quantum order and the existence of topological Majorana excitations, these semiconductor-superconductor structures may have future application as the basic components of a topological quantum computer.

Our proposed non-Abelian system is possibly one of the simplest to study experimentally since it involves neither special materials nor exceptional purity nor the application of a high magnetic field. It is encouraging to note that proximity-induced *s*-wave superconductivity has already been realized in a host InAs semiconductor film,[80,81] which additionally has a sizable spin-orbit coupling. Experimentally, the only new effect that must be introduced to the system is a strong enough Zeeman splitting of the spins. We argue how this can be achieved also via the proximity effect due to a nearby magnetic insulator. It is important to emphasize that when the spin-orbit coupling is of the Rashba type, we require a Zeeman splitting which is perpendicular to the plane of the film. This is because a Zeeman splitting parallel to the film does not produce a gap in the one-electron band structure.[52,53] Inducing a perpendicular splitting by applying a strong perpendicular magnetic field is not convenient because the magnetic field will give rise to unwanted order parameter defects such as vortices. It is for this reason that we propose to induce the Zeeman splitting by the exchange proximity effect of an adjacent magnetic insulator (we ignore the small coupling of the spins in the semiconductor with the actual magnetic field of the magnetic insulator). More recently, it has been shown that, when the spin-orbit coupling also has a component which is of the Dresselhaus type, the appropriate Zeeman splitting can also be induced by applying an in-plane magnetic field.[56] Note that an in-plane magnetic field does not produce unwanted vortex excitations. The one-dimensional version of our system—a semiconducting nanowire—is also a non-Abelian system in the presence of proximity-induced *s*-wave superconductivity and a Zeeman coupling. It is quite exciting that the superconducting proximity effect on an InAs nanowire has already been realized in experiments.[82,83] In this case, the Zeeman coupling can be more easily introduced by applying an external magnetic field parallel to the length of the wire because such a field does produce a gap in the one-electron band structure without producing unwanted excitations in the adjacent superconductor. This obviates the need for a nearby magnetic insulator.[57] In the topological superconducting state of the nanowire (i.e., the Zeeman coupling is above a critical value), there are zero-energy Majorana states localized around the two ends. Such zero-energy states can be revealed by zero-bias conductance peaks in STM tunneling experiments at the ends of the wire. All other contributions to the conductance occur at energies higher than the bulk gap Δ. There will be no such zero-bias peak when the wire is in the topologically trivial *s*-wave superconducting state (i.e., the Zeeman coupling is below the critical value). Such an STM experiment from the semiconducting nanowire will serve as an unambiguous probe for the condensed-matter manifestation of a Majorana fermion mode.

ACKNOWLEDGMENTS

This work is supported by DARPA-QuEST, JQI-NSF-PFC, and LPS-NSA. S.T. acknowledges DOE/EPSCoR Grant No. DE-FG02-04ER-46139 and DARPA-MTO Grant No. FA9550-10-1-0497 for support.

APPENDIX: POWER SERIES FOR THE RASHBA MODEL AT $r>R$

Even though we found an analytic solution for the null vectors of the matrix for $\Delta(r)=0$ in the region $r<R$, we could not find such a solution for $\Delta(r)=\Delta>0$ for $r>R$. In a previous section we claimed without explicit proof that the solution to this equation can be written in terms of a power-series expansion for $\rho(1/r)$. Since we are interested in the solution at large R we expect a power series in $1/R$ to converge. To generate the equation for the power series for ρ it is convenient to shift to a basis where the $1/r=0$ part of the matrix is diagonal,

$$\begin{pmatrix} \eta\left(-\partial_r^2-\frac{1}{4r^2}+2z\partial_r-z^2\right)+V_z-\mu & \pm\Delta+\alpha\left(\partial_r+\frac{1}{2r}-z\right) \\ \mp\Delta-\alpha\left(\partial_r-\frac{1}{2r}-z\right) & \eta\left(-\partial_r^2+\frac{3}{4r^2}+2z\partial_r-z^2\right)-V_z-\mu \end{pmatrix}=A+B, \tag{A1}$$

where

$$A=\begin{pmatrix} -\eta z^2+V_z-\mu & \pm\Delta-z\alpha \\ \mp\Delta+z\alpha & -\eta z^2-V_z-\mu \end{pmatrix}, \tag{A2}$$

$$B=\eta\left(-\partial_r^2-\frac{1}{4r^2}+2z\partial_r\right)+\imath\alpha\sigma_y\partial_r+\alpha\sigma_x/2r-\frac{\eta}{2r^2}\sigma_z. \tag{A3}$$

If S is the matrix of eigenvectors of A then $A=SDS^{-1}$, where D is a diagonal matrix such that $D_{22}=0$ and $D_{11}=\mathrm{Trace}(A)=\eta$. Thus the relevant system of differential equations becomes

$$\left[SDS^{-1}+\eta\left(-\partial_r^2+\frac{1}{4r^2}-\frac{1}{2r^2}\sigma_z+2z\partial_r\right)+\iota\alpha\sigma_y\partial_r+\alpha\sigma_x/2r-\frac{1}{2r^2}\sigma_z\right]\begin{pmatrix}\rho_\uparrow(1/r)\\ \rho_\downarrow(1/r)\end{pmatrix}=0, \tag{A4}$$

$$\begin{pmatrix}\rho_{\uparrow,1}(1/r)\\ \rho_{\downarrow,1}(1/r)\end{pmatrix}=S^{-1}\begin{pmatrix}\rho_\uparrow(1/r)\\ \rho_\downarrow(1/r)\end{pmatrix}, \tag{A5}$$

$$\left[\begin{pmatrix}\eta & 0\\ 0 & 0\end{pmatrix}+\eta\left(-\partial_r^2+\frac{1}{4r^2}-\frac{1}{2r^2}S^{-1}\sigma_zS+2z\partial_r\right)+\alpha S^{-1}(\iota\sigma_y)S\partial_r+\frac{\alpha}{2r}S^{-1}\sigma_xS\right]\begin{pmatrix}\rho_{\uparrow,1}(1/r)\\ \rho_{\downarrow,1}(1/r)\end{pmatrix}=0, \tag{A6}$$

where in the above we note that it is sufficient to provide a series expansion for $\rho_1(1/r)$ since S is independent of r. The matrix S may be written explicitly as

$$S=\begin{pmatrix}\sqrt{b^2-c^2}+b & \sqrt{b^2-c^2}-b\\ -c & c\end{pmatrix}, \tag{A7}$$

where $a=\eta z^2-\mu$, $b=V_z$, and $c=\pm\Delta-\alpha z$.

It is easy to see that our equation is satisfied to order $1/r^2$ by the choice

$$\begin{pmatrix}\rho_{\uparrow,1}(1/r)\\ \rho_{\downarrow,1}(1/r)\end{pmatrix}=\begin{pmatrix}\alpha\dfrac{\sqrt{b^2-c^2}-b}{c\eta}(1/r)\\ 1\end{pmatrix}. \tag{A8}$$

The upper and lower components of the above solutions are different orders in $1/r$. Therefore we redefine our spinor as

$$\begin{pmatrix}\rho_{\uparrow,2}(1/r)\\ \rho_{\downarrow,2}(1/r)\end{pmatrix}=\begin{pmatrix}1 & 0\\ 0 & \dfrac{1}{r}\end{pmatrix}\begin{pmatrix}\rho_{\uparrow,1}(1/r)\\ \rho_{\downarrow,1}(1/r)\end{pmatrix}, \tag{A9}$$

the above solution at lowest order motivates us to modify our ansatz so that the upper and lower component are of the same order in $1/r$ as below

$$M\begin{pmatrix}\rho_{\uparrow,2}(1/r)\\ \rho_{\downarrow,2}(1/r)\end{pmatrix}=0, \tag{A10}$$

where the matrix differential operator M is given by

$$M=\begin{pmatrix}1 & 0\\ 0 & \dfrac{1}{r}\end{pmatrix}\left[\begin{pmatrix}\eta & 0\\ 0 & 0\end{pmatrix}+\eta\left(-\partial_r^2+\frac{1}{4r^2}-\frac{1}{2r^2}S^{-1}\sigma_zS+2z\partial_r\right)+\alpha S^{-1}(\iota\sigma_y)S\partial_r+\frac{\alpha}{2r}S^{-1}\sigma_xS\right]\begin{pmatrix}1 & 0\\ 0 & r\end{pmatrix}. \tag{A11}$$

The terms in the matrix part of the above equation can be separated into two categories. Those that preserve the order of a term $1/r^n$ and those that increase the order of a term to $1/r^{n+1}$. The terms that preserve the order are contained within the matrix below

$$\begin{pmatrix}1 & 0\\ 0 & \dfrac{1}{r}\end{pmatrix}\left[\begin{pmatrix}\eta & 0\\ 0 & 0\end{pmatrix}+\eta(2z\partial_r)+\alpha S^{-1}(\iota\sigma_y)S\partial_r+\frac{\alpha}{2r}S^{-1}\sigma_xS\right]\times\begin{pmatrix}1 & 0\\ 0 & r\end{pmatrix}+\text{higher order} \tag{A12}$$

$$=\begin{pmatrix}\eta & 0\\ 0 & 0\end{pmatrix}+[2\eta z+\alpha S^{-1}(\iota\sigma_y)S]\begin{pmatrix}0 & 0\\ 0 & 1\end{pmatrix}+\alpha\frac{\sqrt{b^2-c^2}-b}{c}\begin{pmatrix}0 & \dfrac{1}{2}+\dfrac{br}{\sqrt{b^2-c^2}}\partial_r\\ 0 & 0\end{pmatrix}+\text{higher order}. \tag{A13}$$

The matrix written explicitly here preserves the order of $1/r^n$ while the rest of the terms generate terms of order $1/r^{n+1}$ or higher. We can check this by applying the above matrix to a spinor proportional to $1/r^n$. The resulting spinor is

$$\left\{\begin{pmatrix}\eta & 0\\ 0 & 0\end{pmatrix}+[2\eta z+\alpha S^{-1}(\iota\sigma_y)S]\begin{pmatrix}0 & 0\\ 0 & 1\end{pmatrix}+\alpha\frac{\sqrt{b^2-c^2}-b}{c}\begin{pmatrix}0 & \dfrac{1}{2}+\dfrac{br}{\sqrt{b^2-c^2}}\partial_r\\ 0 & 0\end{pmatrix}\right\}\frac{1}{r^n}\begin{pmatrix}\rho_\uparrow\\ \rho_\downarrow\end{pmatrix} \tag{A14}$$

$$=\frac{Q_n}{r^n}\begin{pmatrix}\rho_\uparrow\\ \rho_\downarrow\end{pmatrix}, \tag{A15}$$

where

$$Q_n=\left\{\begin{pmatrix}\eta & 0\\ 0 & 0\end{pmatrix}+[2\eta z+\alpha S^{-1}(\iota\sigma_y)S]\begin{pmatrix}0 & 0\\ 0 & 1\end{pmatrix}+\alpha\frac{\sqrt{b^2-c^2}-b}{c}\begin{pmatrix}0 & \dfrac{1}{2}-\dfrac{b(n+1)}{\sqrt{b^2-c^2}}\\ 0 & 0\end{pmatrix}\right\}. \tag{A16}$$

From this it is clear that the action of the matrix differential operator M on the spinor $(\rho_\uparrow,\rho_\downarrow)r^{-n}$ is the nonsingular matrix that acts on the spinor $(\rho_\uparrow,\rho_\downarrow)$ in the above equation.

This fact can be used to create a procedure for generating the power series for $\rho_2(1/r)$ iteratively. To see how this is the case consider the stage after the $(n-1)$th iteration, where the power series has been approximated to

$$\rho_2^{(n-1)}(1/r)=\sum_{j=0}^{n-1}\frac{\rho_2^{(j)}}{r^j}. \tag{A17}$$

To calculate $\rho_2^{(n)}$, we note that

$$0 = M\rho_2^{(n)}(1/r)$$
$$= M\frac{\rho_2^{(n)}}{r^n} + M\rho_2^{(n-1)}(1/r)$$
$$= \frac{Q_n\rho_2^{(n)}}{r^n} + M\rho_2^{(n-1)}(1/r) + o(r^{-(n+1)}). \quad \text{(A18)}$$

Solving the equation to $o(r^{-n})$ yields the iterative relation

$$\rho_2^{(n)} = -Q_n^{-1}\lim_{r\to\infty} r^n M\rho_2^{(n-1)}(1/r). \quad \text{(A19)}$$

As discussed previously, we already have a starting guess for the solution for $n=1$ so that the residue is of order $1/r^2$. Using the nonsingular matrix Q_n we can continue to solve the for the higher-order coefficient by inverting the matrix over the residue. The above argument provides a procedure for how to construct the power series for $\rho(1/r)$ referred to in Eq. (22) of the main body of the text.

[1] J. M. Leinaas and J. Myrheim, Nuovo Cimento Soc. Ital. Fis., B **37**, 1 (1977).
[2] F. Wilczek, Phys. Rev. Lett. **48**, 1144 (1982).
[3] F. Wilczek, *Fractional Statistics and Anyon Superconductivity* (World Scientific, Singapore, 1990).
[4] C. Nayak, S. H. Simon, A. Stern, M. Freedman, and S. Das Sarma, Rev. Mod. Phys. **80**, 1083 (2008).
[5] A. Yu. Kitaev, Ann. Phys. **303**, 2 (2003).
[6] M. H. Freedman, M. J. Larsen, and Z. A. Wang, Commun. Math. Phys. **227**, 605 (2002).
[7] E. Majorana, Nuovo Cimento **5**, 171 (1937).
[8] F. Wilczek, Nat. Phys. **5**, 614 (2009).
[9] A. Stern, Nature (London) **464**, 187 (2010).
[10] G. Moore and N. Read, Nucl. Phys. B **360**, 362 (1991).
[11] C. Nayak and F. Wilczek, Nucl. Phys. B **479**, 529 (1996).
[12] N. Read and D. Green, Phys. Rev. B **61**, 10267 (2000).
[13] S. Das Sarma, M. Freedman, and C. Nayak, Phys. Rev. Lett. **94**, 166802 (2005).
[14] A. Stern and B. I. Halperin, Phys. Rev. Lett. **96**, 016802 (2006).
[15] P. Bonderson, A. Kitaev, and K. Shtengel, Phys. Rev. Lett. **96**, 016803 (2006).
[16] P. Bonderson, K. Shtengel, and J. K. Slingerland, Phys. Rev. Lett. **97**, 016401 (2006).
[17] B. Rosenow, B. I. Halperin, S. H. Simon, and A. Stern, Phys. Rev. Lett. **100**, 226803 (2008).
[18] M. M. Salomaa and G. E. Volovik, Phys. Rev. B **37**, 9298 (1988).
[19] D. A. Ivanov, Phys. Rev. Lett. **86**, 268 (2001).
[20] A. Stern, F. von Oppen, and E. Mariani, Phys. Rev. B **70**, 205338 (2004).
[21] S. Das Sarma, C. Nayak, and S. Tewari, Phys. Rev. B **73**, 220502(R) (2006).
[22] S. Tewari, S. Das Sarma, and D. H. Lee, Phys. Rev. Lett. **99**, 037001 (2007).
[23] S. Tewari, S. Das Sarma, C. Nayak, C. W. Zhang, and P. Zoller, Phys. Rev. Lett. **98**, 010506 (2007).
[24] S. Tewari, C. W. Zhang, S. Das Sarma, C. Nayak, and D.-H. Lee, Phys. Rev. Lett. **100**, 027001 (2008).
[25] C.-H. Cheng and S.-K. Yip, Phys. Rev. Lett. **95**, 070404 (2005).
[26] V. Gurarie, L. Radzihovsky, and A. V. Andreev, Phys. Rev. Lett. **94**, 230403 (2005).
[27] V. Gurarie and L. Radzihovsky, Phys. Rev. B **75**, 212509 (2007).
[28] G. E. Volovik, Pis'ma Zh. Eksp. Teor. Fiz. **91**, 61 (2010).
[29] M. Silaev and G. Volovik, J. Low Temp. Phys. **161**, 420 (2010).
[30] Y. Nishida, Phys. Rev. D **81**, 074004 (2010).
[31] M. Wimmer, A. Akhmerov, M. Medvedyeva, J. Tworzydlo, and C. Beenakker, Phys. Rev. Lett. **105**, 046803 (2010).
[32] A. Y. Kitaev, Ann. Phys. (N.Y.) **321**, 2 (2006).
[33] H. Yao and S. A. Kivelson, Phys. Rev. Lett. **99**, 247203 (2007).
[34] S. Trebst, P. Werner, M. Troyer, K. Shtengel, and C. Nayak, Phys. Rev. Lett. **98**, 070602 (2007).
[35] L.-M. Duan, E. Demler, and M. D. Lukin, Phys. Rev. Lett. **91**, 090402 (2003).
[36] C. W. Zhang, V. W. Scarola, S. Tewari, and S. Das Sarma, Proc. Natl. Acad. Sci. U.S.A. **104**, 18415 (2007).
[37] L. Fu and C. L. Kane, Phys. Rev. Lett. **100**, 096407 (2008).
[38] R. Jackiw and P. Rossi, Nucl. Phys. B **190**, 681 (1981).
[39] L. Fu and C. L. Kane, Phys. Rev. Lett. **102**, 216403 (2009).
[40] A. R. Akhmerov, J. Nilsson, and C. W. J. Beenakker, Phys. Rev. Lett. **102**, 216404 (2009).
[41] L. Fu, Phys. Rev. Lett. **104**, 056402 (2010).
[42] J. Sau, R. Lutchyn, S. Tewari, and S. Das Sarma, Phys. Rev. B **82**, 094522 (2010).
[43] T. D. Stanescu, J. D. Sau, R. M. Lutchyn, and S. Das Sarma, Phys. Rev. B **81**, 241310 (2010).
[44] J. Nilsson and A. R. Akhmerov, Phys. Rev. B **81**, 205110 (2010).
[45] K. T. Law, P. A. Lee, and T. K. Ng, Phys. Rev. Lett. **103**, 237001 (2009).
[46] J. Nilsson, A. R. Akhmerov, and C. W. J. Beenakker, Phys. Rev. Lett. **101**, 120403 (2008).
[47] Y. Tanaka, T. Yokoyama, and N. Nagaosa, Phys. Rev. Lett. **103**, 107002 (2009).
[48] P. Lee, arXiv:0907.2681 (unpublished).
[49] X. Qi, T. Hughes, and S. Zhang, arXiv:1003.5448 (unpublished).
[50] C. W. Zhang, S. Tewari, R. M. Lutchyn, and S. Das Sarma, Phys. Rev. Lett. **101**, 160401 (2008).
[51] M. Sato, Y. Takahashi, and S. Fujimoto, Phys. Rev. Lett. **103**, 020401 (2009).
[52] J. D. Sau, R. M. Lutchyn, S. Tewari, and S. Das Sarma, Phys. Rev. Lett. **104**, 040502 (2010).
[53] S. Tewari, J. D. Sau, and S. Das Sarma, Ann. Phys. **325**, 219 (2010).
[54] R. Jackiw and C. Rebbi, Phys. Rev. D **13**, 3398 (1976).
[55] R. Jackiw and J. R. Schrieffer, Nucl. Phys. B **190**, 253 (1981).
[56] J. Alicea, Phys. Rev. B **81**, 125318 (2010).
[57] R. M. Lutchyn, J. D. Sau, and S. Das Sarma, Phys. Rev. Lett. **105**, 077001 (2010).
[58] Y. E. Kraus, A. Auerbach, H. A. Fertig, and S. H. Simon, Phys. Rev. Lett. **101**, 267002 (2008).
[59] Y. E. Kraus, A. Auerbach, H. A. Fertig, and S. H. Simon, Phys.

Rev. B **79**, 134515 (2009).
[60] M. Cheng, R. M. Lutchyn, V. Galitski, and S. Das Sarma, Phys. Rev. Lett. **103**, 107001 (2009).
[61] P. Ghosh, J. Sau, S. Tewari, and S. Das Sarma, Phys. Rev. B **82**, 184525 (2010).
[62] G. E. Volovik, Zh. Eksp. Teor. Fiz. **94**, 123 (1988) [Sov. Phys. JETP **67**, 1804 (1988)].
[63] G. E. Volovik and V. M. Yakovenko, J. Phys.: Condens. Matter **1**, 5263 (1989).
[64] V. M. Yakovenko, Phys. Rev. Lett. **65**, 251 (1990).
[65] R. Roy, Phys. Rev. Lett. **105**, 186401 (2010).
[66] B. S. Chandrasekhar, Appl. Phys. Lett. **1**, 7 (1962).
[67] A. M. Clogston, Phys. Rev. Lett. **9**, 266 (1962).
[68] M. Hasan and C. Kane, Rev. Mod. Phys. **82**, 3045 (2010).
[69] J. Sau and S. Tewari, S. Das Sarma, arXiv:1004.4702 (unpublished).
[70] I. Serban, B. Beri, A. Akhmerov, and C. Beenakker, Phys. Rev. Lett. **104**, 147001 (2010).
[71] F. Nolting, A. Scholl, J. Stöhr, J. W. Seov, J. Fompeyrine, H. Siegwart, J.-P. Locquet, S. Anders, J. Lüning, E. E. Fullerton, M. F. Toney, M. R. Scheinfein, and H. A. Padmore, Nature (London) **405**, 767 (2000).
[72] J. Nogués and I. K. Schuller, J. Magn. Magn. Mater. **192**, 203 (1999).
[73] Y. Oreg, G. Refael, and F. von Oppen, arXiv:1003.1145 (unpublished).
[74] K. Sengupta, I. Zutic, H. J. Kwon, V. M. Yakovenko, and S. Das Sarma, Phys. Rev. B **63**, 144531 (2001).
[75] C. J. Bolech and E. Demler, Phys. Rev. Lett. **98**, 237002 (2007).
[76] H. Haug and A. Jauho, *Quantum Kinetics in Transport and Optics in Semiconductors*, Springer Series in Solid State Sciences (Springer-Verlag, Berlin, Heidelberg 2008).
[77] J. C. Quateman, Phys. Rev. B **34**, 1948 (1986).
[78] S. Bravyi, Phys. Rev. A **73**, 042313 (2006).
[79] P. Bonderson, S. Das Sarma, M. Freedman, and C. Nayak, Phys. Rev. Lett. **105**, 177002 (2010).
[80] A. Chrestin, T. Matsuyama, and U. Merkt, Phys. Rev. B **55**, 8457 (1997).
[81] F. Giazotto, K. Grove-Rasmussen, R. Fazio, F. Beltram, E. H. Linfield, and D. A. Ritchie, J. Supercond. **17**, 317 (2004).
[82] Y. J. Doh, J. A. van Dam, A. L. Roest, E. P. A. M. Bakkers, L. P. Kouwenhoven, and S. De Franceschi, Science **309**, 272 (2005).
[83] C. Caroli, P. G. De Gennes, and J. Matricon, Phys. Lett. **9**, 307 (1964).